J. Fluid Mech. (2004), *vol.* 499, *pp.* 345–380. © 2004 Cambridge University Press
DOI: 10.1017/S0022112003007122 Printed in the United Kingdom

Steady streaming from an oblate spheroid due to vibrations along its axis

By A. Y. REDNIKOV AND S. S. SADHAL

Aerospace & Mechanical Engineering, University of Southern California, Los Angeles, CA 90089-1453, USA

(Received 1 August 2002 and in revised form 7 September 2003)

Steady (acoustic) streaming around a rigid oblate spheroid is studied in the incompressible limit when the fluid medium and the particle are in a small-amplitude high-frequency relative oscillatory motion along the symmetry axis of the spheroid. The inner (inside the thin Stokes shear-wave layer) and outer streaming patterns are analysed. A solution for the outer streaming is obtained analytically for small Reynolds numbers. At large Reynolds numbers, a boundary-layer consideration is carried out. Steady streaming in the disk limit, as approached within the family of oblate spheroids, is systematically investigated in the large Reynolds number case, and qualitative implications for shapes other than oblate spheroidal are discussed.

1. Introduction

The phenomenon of acoustic streaming manifests itself by the appearance of a steady flow component in a primarily oscillatory flow, such as an acoustic wave, and is due to the nonlinearity of the laws governing fluid motion as well as the dissipative factors, such as viscosity, operating therein (Rayleigh 1883; Andrade 1931; Schlichting 1932; see also the reviews by Nyborg 1965 and Riley 2001 for details). Typically, and this is assumed in the present paper, the primary oscillatory flow is characterized by a small amplitude and high frequency. Namely, the amplitude of the fluid element displacement is small compared to the length scale of the problem, which may be the size of the particle involved or the acoustic wavelength. The frequency is high on the viscous time scale.

Despite the commonly used name, the same phenomenon occurs equally well in genuinely incompressible situations, and in this case the term 'steady streaming' seems more appropriate (Riley 2001). Of the two streaming mechanisms pointed out by Riley (2001), only the Rayleigh one is relevant in the incompressible case. According to it, the steady streaming originates in a thin shear-wave layer (the Stokes boundary layer) at a solid boundary to which the oscillatory vorticity is confined in the high-frequency limit. However, the streaming itself cannot be confined to the Stokes layer (inner streaming) and develops into the main body of the fluid (outer streaming). Mathematically, as the Stokes layer is asymptotically thin compared to the length scale of the problem, the outer streaming formally appears to be caused by an effective slip velocity at the boundary. The latter represents the inner streaming that persists (and cannot be made to vanish) at the outer edge of the Stokes layer.

A significant part of the literature on the subject is devoted to the streaming from particles in the incompressible case (see Riley 2001 and references therein). An exemplar for such a study is put forth by Riley (1966), who considers a sphere

https://doi.org/10.1017/S0022112003007122 Published online by Cambridge University Press

which oscillates translationally relative to the fluid medium. This class of problems does not necessarily require any explicit acoustic context, as is demonstrated by the experiments carried out by Davidson & Riley (1972) and Amin & Riley (1990) on steady streaming in an incompressible liquid. Nevertheless, another important application is to particles held against gravity in acoustic levitators, provided that the particle is sufficiently small compared to the acoustic wavelength. In this case, incompressibity is valid locally in the vicinity of the particle to the leading order in the parameter $kl \ll 1$, where k is the wavenumber and l is the particle size. Higher-order terms in kl for a sphere may also be analysed, as e.g. in Lee & Wang (1990) and Zhao, Sadhal & Trinh (1999*a*). Yarin *et al.* (1999) assume neither kl being small, nor the particle being spherical, but in what concerns acoustic streaming their consideration is limited to the Stokes layer.

The present paper deals with the steady streaming, in the incompressible limit, around a rigid oblate spheroid that performs translational oscillations relative to the fluid medium along its symmetry axis. The motivation for such a study is two-fold. On the one hand, liquid drops are known to be squeezed to an oblate shape, quite close to an oblate spheroid, when levitated in acoustic levitators at sufficiently high intensities of the sound field (e.g. Lee, Anikumar & Wang 1994; Yarin, Pfaffenlehn & Tropea 1998). Due to their large density and dynamic viscosity compared to those of the surrounding air, the drops may behave to a high degree as rigid bodies regarding streaming. In particular, the influence of the acoustically induced internal circulation in a drop on the steady streaming in the air can be estimated using the results of Zhao, Sadhal & Trinh 1999*b* and Yarin *et al.* (1999). On the other hand, the study of the streaming around a body more complex than a sphere may have intrinsic importance, especially in view of our intention to consider the disk limit. The choice of the oblate spheroid for this purpose is convenient in view of the availability of the oblate spheroidal coordinate system.

In § 2 the problem is formulated and assumptions are stated. In § 3 we consider the primary oscillatory flow. The inner steady streaming (in the Stokes layer) is analysed in § 4, and the effective slip velocity is found. Also, § 4 contains a first evaluation, based upon the Stokes layer results, of the streaming characteristic scaling in the disk limit, as the aspect ratio of the oblate spheroid tends to zero. Problem formulation for the outer streaming is consolidated in § 5. For a small streaming Reynolds number, the solution for the outer streaming is constructed analytically by means of the Stokes approximation in § 6. The opposite case, of a large streaming Reynolds number, is considered numerically in § 7 with the help of the boundary-layer approximation. In § 8, still within the boundary-layer approximation, we study the outer streaming in the disk limit. Finally, results are summarized in § 9.

2. Formulation

2.1. *Statement of the problem and assumptions*

Consider a rigid oblate spheroid placed in an unbounded incompressible fluid medium. The particle and the medium are in a small-amplitude high-frequency translational harmonic oscillatory motion relative to each other, with the velocity amplitude U_∞ and the frequency ω, along the symmetry axis of the spheroid. We work in the reference frame fixed to the particle, where the latter is at rest while the fluid motion far away from it is described by an oscillatory uniform parallel flow. Our goal here is to describe the time-independent flow component (mean flow or steady streaming) that develops on such an oscillatory background. While we focus on the Eulerian

https://doi.org/10.1017/S0022112003007122 Published online by Cambridge University Press

mean flow in the above-mentioned frame of reference, we will later discuss whether the Lagrangian mean flow (Nyborg 1965; Riley 2001) is in any way different and whether the result changes in other reference frames of possible physical meaning which oscillate relative to the chosen one.

Let l be the length scale of the problem. It is of order of the size of the spheroid, but will be specified later. Choosing l, $1/\omega$, U_∞ and $\rho U_\infty \omega l$ (ρ is the fluid density) as the units of length, time, velocity and pressure, respectively, the dimensionless Navier–Stokes equations can be written as

$$\nabla \cdot \boldsymbol{v} = 0, \tag{1}$$

$$\frac{\partial \boldsymbol{v}}{\partial t} - \varepsilon \boldsymbol{v} \times [\nabla \times \boldsymbol{v}] = -\nabla \left(p + \tfrac{1}{2}\varepsilon |\boldsymbol{v}|^2 \right) - \frac{1}{M^2} \nabla \times [\nabla \times \boldsymbol{v}] \tag{2}$$

with

$$\varepsilon = \frac{U_\infty}{\omega l}, \quad M^2 = \frac{\omega l^2}{\nu}. \tag{3}$$

Here t is the time; $\boldsymbol{v}$ and p are the velocity and hydrodynamic pressure fields; and ν is the kinematic viscosity. The mathematical formulation is completed by imposing non-penetration and no-slip boundary conditions ($\boldsymbol{v} = \boldsymbol{0}$) at the surface of the spheroid and uniform parallel oscillatory flow ($\boldsymbol{v} \sim \boldsymbol{e}_z \cos t$, with $\boldsymbol{e}_z$ being the unit vector along the symmetry axis, which is taken as the z-axis) far away from it.

The problem is treated under the assumptions of small amplitude and high frequency of the oscillations. More precisely, the amplitude of fluid-element displacement in the oscillatory flow is much smaller than the typical length scale l. Thus, $\varepsilon \ll 1$. The frequency ω is high with respect to the viscous time scale, l^2/ν; hence $M \gg 1$. Thus, the asymptotic case treated here corresponds to

$$\varepsilon \ll 1, \quad M \gg 1. \tag{4}$$

The analysis is focused on obtaining the leading-order mean flow around the oblate spheroid.

In the high-frequency limit, the primary oscillatory flow assumes a boundary-layer structure. Viscous effects are important and vorticity is present only in a thin shear-wave layer (the Stokes layer) at the body surface, of relative thickness $O(1/M)$. Outside that layer, in the main bulk of the fluid, the leading-order oscillatory flow is irrotational. Such a two-scale structure of the oscillatory flow is also enforced on the steady streaming, for the latter is generated from the former by means of the nonlinearity in the Navier–Stokes equations. The generation, but not the streaming itself, is limited to the Stokes layer, where the oscillatory vorticity is not zero. In the asymptotic approach we follow here, the whole flow region is subdivided into two subregions – the main bulk and the Stokes layer. Solutions are sought separately in each of them with the condition of asymptotic matching imposed.

2.2. *Reformulation in the oblate spheroidal coordinates and in terms of stream function*

The problem is treated in the oblate spheroidal coordinates (see e.g. Happel & Brenner 1965) that include our physical oblate spheroid as a coordinate surface. It proves more convenient here to use modified oblate spheroidal coordinates, denoted as $\{\mu, \lambda, \phi\}$, where ϕ is the azimuthal angle. In terms of the cylindrical coordinates $\{z, \varrho, \phi\}$, with ϱ being the distance from the polar axis, these are defined as follows:

$$z = c\,\lambda\,\mu, \quad \varrho = c\,(1+\lambda^2)^{1/2}\,(1-\mu^2)^{1/2} \tag{5}$$

https://doi.org/10.1017/S0022112003007122 Published online by Cambridge University Press

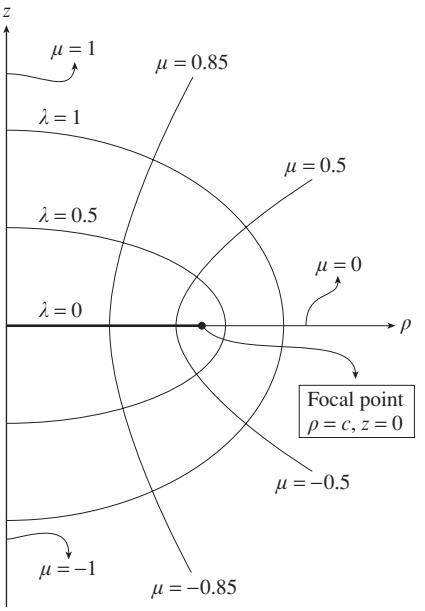


FIGURE 1. The oblate spheroidal coordinates, equation (5).

where the coordinates lie in the ranges $0 \leqslant \lambda < \infty$, $-1 \leqslant \mu \leqslant 1$, $0 \leqslant \phi < 2\pi$ to cover all the space once. The parameter c is the focal radius. The coordinate system (5) is schematically depicted in figure 1.

The coordinate surfaces $\lambda = \text{const}$ form a family of confocal oblate spheroids. Let us define $\lambda = \lambda_0$ as corresponding to the physical oblate spheroid the streaming around which is studied here. Its major (equatorial) and minor (polar) radii are

$$a = c\left(1+\lambda_0^2\right)^{1/2}, \quad b = c\lambda_0, \tag{6}$$

respectively. The aspect ratio of the spheroid is a function of λ_0 only:

$$b/a = \lambda_0 \big/ \left(1+\lambda_0^2\right)^{1/2}. \tag{7}$$

The value of c is determined by the choice of the length scale l (see §2.1). If l is chosen to be the major radius of the spheroid, then

$$a \equiv 1, \quad c = 1 \big/ \left(1+\lambda_0^2\right)^{1/2}. \tag{8}$$

Another reasonable candidate for l is the radius of the sphere with the same volume as the spheroid. In this case, $a^2 b \equiv 1$ and $c = 1/(\lambda_0(1+\lambda_0^2))^{1/3}$. In the present paper, while keeping c unspecified throughout analytical manipulations, we will use (8) whenever particular numerical values are provided (including on the plots).

Given the axial symmetry, it may be convenient to work in terms of the stream function ψ. The μ and λ velocity components are expressed as (e.g. Happel & Brenner 1965; see also Appendix A)

$$v_\mu = \frac{1}{c^2(1-\mu^2)^{1/2}(\lambda^2+\mu^2)^{1/2}} \frac{\partial \psi}{\partial \lambda}, \quad v_\lambda = -\frac{1}{c^2(1+\lambda^2)^{1/2}(\lambda^2+\mu^2)^{1/2}} \frac{\partial \psi}{\partial \mu}. \tag{9}$$

Equation (1) is thereby identically satisfied. In equation (2), the pressure is eliminated by taking the curl. The result is subsequently cast in terms of the stream

https://doi.org/10.1017/S0022112003007122 Published online by Cambridge University Press

function to yield (see Appendix A for more details)

$$\frac{\partial \mathrm{E}^2\psi}{\partial t} + \varepsilon\, \mathrm{N}(\psi, \mathrm{E}^2\psi) = \frac{1}{M^2}\mathrm{E}^4\psi \tag{10}$$

with the bilinear operator N defined as

$$\mathrm{N}(f,\ g) = \frac{1}{c^3(\lambda^2+\mu^2)}\left\{\frac{\partial(f,g)}{\partial(\lambda,\mu)} + 2\left[\frac{\mu}{1-\mu^2}\frac{\partial f}{\partial \lambda} + \frac{\lambda}{1+\lambda^2}\frac{\partial f}{\partial \mu}\right] g\right\}$$

where f and g are arbitrary functions, and with the operators

$$\mathrm{E}^2 = \frac{1}{c^2(\lambda^2+\mu^2)}\left[(1+\lambda^2)\frac{\partial^2}{\partial\lambda^2} + (1-\mu^2)\frac{\partial^2}{\partial\mu^2}\right], \qquad \mathrm{E}^4 = \mathrm{E}^2\mathrm{E}^2.$$

Next, we turn to the boundary conditions. The oscillatory uniform parallel flow at infinity is $\psi = \frac{1}{2}\varrho^2 \exp(\mathrm{i}t)$, and with (5) we obtain

$$\lambda \to \infty\colon \quad \psi \sim \tfrac{1}{2}c^2(1+\lambda^2)(1-\mu^2)\mathrm{e}^{\mathrm{i}t}. \tag{11}$$

The non-penetration and no-slip conditions at the surface of the oblate spheroid can be written as

$$\lambda = \lambda_0\colon \quad \psi = \frac{\partial\psi}{\partial\lambda} = 0. \tag{12}$$

Thus, the problem for the stream function is given by (10)–(12).

It might be useful to notice that the case of a spherical particle and the corresponding results in spherical coordinates $\{r, \theta, \phi\}$ are recovered in the limit

$$c \to 0, \quad \lambda \to \infty, \quad \lambda_0 \to \infty, \quad c\lambda \to r, \quad c\lambda_0 \to 1, \quad \mu \to \cos\theta, \tag{13}$$

where $r = 1$ gives the surface of the sphere.

2.3. *Formulation for the Stokes layer*

When considering the Stokes layer, it is convenient to recast equation (10) in the appropriate Stokes-layer variables. As the layer thickness is $O(1/M)$, we write

$$\Lambda = M(\lambda - \lambda_0), \quad \Psi = M\psi, \tag{14}$$

so that both Λ and Ψ are $O(1)$ inside the layer. Upon using (14) in (10), we keep only the leading-order terms in both the linear and nonlinear parts of the equation, which will suffice for the purposes of the present paper. Accordingly, the Stokes-layer version of equation (10) can be written as

$$\frac{\partial}{\partial t}\frac{\partial^2\Psi}{\partial\Lambda^2} + \frac{\varepsilon}{c^3\left(\lambda_0^2+\mu^2\right)}\left[\frac{\partial\Psi}{\partial\Lambda}\frac{\partial^3\Psi}{\partial\mu\partial\Lambda^2} - \frac{\partial\Psi}{\partial\mu}\frac{\partial^3\Psi}{\partial\Lambda^3}\right] + 2\varepsilon\left[-\frac{\mu}{c^3\left(\lambda_0^2+\mu^2\right)^2} + \frac{\mu}{1-\mu^2}\frac{1}{c^3\left(\lambda_0^2+\mu^2\right)}\right]\frac{\partial\Psi}{\partial\Lambda}\frac{\partial^2\Psi}{\partial\Lambda^2} = \frac{1+\lambda_0^2}{c^2\left(\lambda_0^2+\mu^2\right)}\frac{\partial^4\Psi}{\partial\Lambda^4}. \tag{15}$$

Equation (15) can be integrated once with respect to Λ to yield

$$\frac{\partial}{\partial t}\frac{\partial\Psi}{\partial\Lambda} + \frac{\varepsilon}{c^3\left(\lambda_0^2+\mu^2\right)}\left[\frac{1}{2}\frac{\partial}{\partial\mu}\left(\frac{\partial\Psi}{\partial\Lambda}\right)^2 - \frac{\partial\Psi}{\partial\mu}\frac{\partial^2\Psi}{\partial\Lambda^2}\right] + \varepsilon\left[-\frac{\mu}{c^3\left(\lambda_0^2+\mu^2\right)^2} + \frac{\mu}{1-\mu^2}\frac{1}{c^3\left(\lambda_0^2+\mu^2\right)}\right]\left(\frac{\partial\Psi}{\partial\Lambda}\right)^2 = -\Pi(t,\mu) + \frac{1+\lambda_0^2}{c^2\left(\lambda_0^2+\mu^2\right)}\frac{\partial^3\Psi}{\partial\Lambda^3}, \tag{16}$$

https://doi.org/10.1017/S0022112003007122 Published online by Cambridge University Press

where Π is a 'constant' of integration, which is a function of both t and μ.

Rather than Λ, it would be advantageous to use the variable

$$Y = \frac{c\left(\lambda_0^2+\mu^2\right)^{1/2}}{\left(1+\lambda_0^2\right)^{1/2}} M(\lambda-\lambda_0) = \frac{c\left(\lambda_0^2+\mu^2\right)^{1/2}}{\left(1+\lambda_0^2\right)^{1/2}} \Lambda \tag{17}$$

that conveniently removes the factor at the highest derivative in (16). Notice that, to leading order and up to the scaling with M, the coordinate Y measures the normal distance from the spheroid. Indeed, the multiplier (17) can be recognized as the appropriate metric coefficient (see Appendix A). Using (17) and implying the appropriate redefinition of Π, equation (16) becomes

$$\frac{\partial}{\partial t}\frac{\partial \Psi}{\partial Y} + \frac{\varepsilon}{c^2\left(1+\lambda_0^2\right)^{1/2}\left(\lambda_0^2+\mu^2\right)^{1/2}}\left[\frac{1}{2}\frac{\partial}{\partial \mu}\left(\frac{\partial \Psi}{\partial Y}\right)^2 - \frac{\partial \Psi}{\partial \mu}\frac{\partial^2 \Psi}{\partial Y^2} + \frac{\mu}{1-\mu^2}\left(\frac{\partial \Psi}{\partial Y}\right)^2\right] = -\Pi(t,\mu) + \frac{\partial^3 \Psi}{\partial Y^3}, \tag{18}$$

which is finally the equation used in the Stokes layer. Boundary conditions (12) are rewritten as

$$Y = 0: \quad \Psi = \frac{\partial \Psi}{\partial Y} = 0. \tag{19}$$

The formulation is completed by the condition of matching between solutions in the bulk of the fluid and in the Stokes layer, which can schematically be written as

$$\psi(t,\mu,\lambda)\big|_{\lambda\to\lambda_0} \sim \frac{1}{M}\Psi(t,\mu,Y)\big|_{Y\to\infty}. \tag{20}$$

The function $\Pi(t,\mu)$ is determined in the solution process. It is related to the pressure distribution in the Stokes layer, which is constant (to leading order) across the layer.

2.4. *The form of the solution; the unsteady and steady parts*

The flow field is represented as a sum of the unsteady (oscillatory, fluctuating) and steady (mean, time-averaged, time-independent) parts:

$$f = f^{(u)} + \varepsilon\, f^{(s)}, \tag{21}$$

where the symbol f stands for any flow characteristic, such as ψ, Ψ, v_μ, etc. The superscripts (u) and (s) refer to unsteady and 'steady', respectively. The unsteady part is an $O(1)$ quantity by definition. The steady part is generated by nonlinearity in the Navier–Stokes equations and is expected to be of $O(\varepsilon)$ here. By putting ε explicitly into (21) we obtain $f^{(s)} = O(1)$.

Each of the functions $f^{(u)}$ and $f^{(s)}$ is in turn to be expanded in an asymptotic series with the two small parameter of the problem, ε and $1/M$. However, in the present paper, unless the contrary is stated, we limit ourselves to the leading-order results for both the steady and unsteady parts, and no further expansions are developed.

3. Primary oscillatory flow

It follows from (10)–(12) under the assumptions (4) that the leading-order problem for the oscillatory part $\psi^{(u)}$ (equation (21)) in the main bulk of the fluid is

$$\mathrm{E}^2\psi^{(u)} = 0, \tag{22}$$

$$\lambda \to \lambda_0: \quad \psi^{(u)} \sim \tfrac{1}{2}c^2(1+\lambda^2)(1-\mu^2)\,\mathrm{e}^{\mathrm{i}t}; \qquad \lambda = \lambda_0: \quad \psi^{(u)} = 0. \tag{23}$$

https://doi.org/10.1017/S0022112003007122 Published online by Cambridge University Press

Equation (22) states that the primary oscillatory flow is irrotational. The no-slip condition is lost in (23) and will be accommodated in the Stokes layer. The solution of (22) and (23) is sought in the form

$$\psi^{(u)} = g(\lambda)(1-\mu^2)\,\mathrm{e}^{\mathrm{i}t} \tag{24}$$

which upon using in (22) leads to

$$(1+\lambda^2)\frac{\mathrm{d}^2 g}{\mathrm{d}\lambda^2} - 2g = 0.$$

This can be integrated once to yield

$$(1+\lambda^2)\frac{\mathrm{d}g}{\mathrm{d}\lambda} - 2\lambda g = C_1 \qquad \text{or} \qquad \frac{\mathrm{d}}{\mathrm{d}\lambda}\left(\frac{g}{1+\lambda^2}\right) = \frac{C_1}{(1+\lambda^2)^2}$$

and the general solution is

$$g(\lambda) = \tfrac{1}{2}C_1[\lambda - (1+\lambda^2)\mathrm{arccot}(\lambda)] + C_2(1+\lambda^2). \tag{25}$$

Upon finding the coefficients C_1 and C_2 by requiring (24) with (25) to satisfy the boundary conditions (23), we finally obtain

$$\psi^{(u)} = \tfrac{1}{2}c^2\left[1+\lambda^2 - \left(1+\lambda_0^2\right)\frac{(1+\lambda^2)\mathrm{arccot}(\lambda) - \lambda}{\left(1+\lambda_0^2\right)\mathrm{arccot}(\lambda_0) - \lambda_0}\right](1-\mu^2)\,\mathrm{e}^{\mathrm{i}t}. \tag{26}$$

Turning to the Stokes layer, we apply (18)–(20) to the fluctuating part $\Psi^{(u)}$. The matching condition (20), which now involves $\psi^{(u)}$ and $\Psi^{(u)}$, takes (26) into account. The following problem for $\Psi^{(u)}$ results:

$$\frac{\partial}{\partial t}\frac{\partial \Psi^{(u)}}{\partial Y} = -\Pi^{(u)}(t,\mu) + \frac{\partial^3 \Psi^{(u)}}{\partial Y^3}, \tag{27}$$

$$Y \to \infty: \quad \Psi^{(u)} \sim A\,\frac{\left(1+\lambda_0^2\right)^{1/2}}{\left(\lambda_0^2+\mu^2\right)^{1/2}}\,Y\,(1-\mu^2)\,\mathrm{e}^{\mathrm{i}t}, \tag{28}$$

$$Y = 0: \quad \Psi^{(u)} = \frac{\partial \Psi^{(u)}}{\partial Y} = 0, \tag{29}$$

where

$$A = \frac{c}{\left(1+\lambda_0^2\right)\mathrm{arccot}(\lambda_0) - \lambda_0}. \tag{30}$$

Let us mention for further reference that $A = 3/2$ in the sphere limit (13), and $A = 2c/\pi$ in the disk limit $\lambda_0 \to 0$.

We observe that a solution to (27)–(29) exists only if

$$\Pi^{(u)} = -\mathrm{i}A\,\frac{\left(1+\lambda_0^2\right)^{1/2}}{\left(\lambda_0^2+\mu^2\right)^{1/2}}\,(1-\mu^2)\,\mathrm{e}^{\mathrm{i}t}$$

and the solution is

$$\Psi^{(u)} = A\,\frac{\left(1+\lambda_0^2\right)^{1/2}}{\left(\lambda_0^2+\mu^2\right)^{1/2}}\left\{Y - \frac{1}{\sqrt{\mathrm{i}}}[1-\mathrm{e}^{-\sqrt{\mathrm{i}}Y}]\right\}(1-\mu^2)\,\mathrm{e}^{\mathrm{i}t} \tag{31}$$

where $\sqrt{\mathrm{i}} = (1+\mathrm{i})/\sqrt{2}$.

https://doi.org/10.1017/S0022112003007122 Published online by Cambridge University Press

Thus, the primary oscillatory flow is given by equation (26) in the main bulk of the fluid, and by equation (31) in the Stokes layer. Now we proceed to the steady part of the flow.

4. Steady streaming in the Stokes layer

First we turn to the steady flow in the Stokes layer. Substituting (21) into (18), with $f \equiv \Psi$, taking the time average of the equation, and retaining only the leading-order terms, we obtain

$$\frac{1}{c^2\left(1+\lambda_0^2\right)^{1/2}\left(\lambda_0^2+\mu^2\right)^{1/2}}\left\langle \frac{1}{2}\frac{\partial}{\partial\mu}\left(\frac{\partial\Psi^{(u)}}{\partial Y}\right)^2 - \frac{\partial\Psi^{(u)}}{\partial\mu}\frac{\partial^2\Psi^{(u)}}{\partial Y^2} + \frac{\mu}{1-\mu^2}\left(\frac{\partial\Psi^{(u)}}{\partial Y}\right)^2\right\rangle = -\Pi^{(s)}(\mu) + \frac{\partial^3\Psi^{(s)}}{\partial Y^3}. \quad (32)$$

The time-averaged nonlinear terms on the left-hand side of (32) represent the action of the Reynolds stresses that generates the steady streaming. They are explicitly calculated using the expression for $\Psi^{(u)}$, equation (31). The solution should satisfy the non-penetration and the no-slip conditions at the surface,

$$Y = 0: \quad \Psi^{(s)} = \frac{\partial\Psi^{(s)}}{\partial Y} = 0.$$

Also, as $Y \to \infty$, it should possess the minimal possible singularity (Riley 1965). By allowing the $O(Y^3)$ terms in $\Psi^{(s)}$ to vanish, we obtain

$$\Pi^{(s)}(\mu) = A^2\frac{\left(1+\lambda_0^2\right)^{3/2}\mu(1-\mu^2)}{2c^2\left(\lambda_0^2+\mu^2\right)^{5/2}}$$

and the solution is

$$\Psi^{(s)} = A^2\frac{\left(1+\lambda_0^2\right)^{1/2}\mu\,(1-\mu^2)}{\sqrt{2}\,c^2\left(\lambda_0^2+\mu^2\right)^{3/2}}\left[f_1\left(\frac{Y}{\sqrt{2}}\right)\frac{1-\mu^2}{\lambda_0^2+\mu^2} + f_2\left(\frac{Y}{\sqrt{2}}\right)\right] \quad (33)$$

with

$$f_1(z) = z\,\mathrm{e}^{-z}\sin z + 3\mathrm{e}^{-z}\cos z + 2\mathrm{e}^{-z}\sin z + \tfrac{1}{4}\mathrm{e}^{-2z} + \tfrac{3}{2}z - \tfrac{13}{4},$$
$$f_2(z) = 2\,z\,\mathrm{e}^{-z}\sin z + 5\mathrm{e}^{-z}\cos z + 3\mathrm{e}^{-z}\sin z + \tfrac{1}{4}\mathrm{e}^{-2z} + \tfrac{5}{2}z - \tfrac{21}{4}.$$

Despite the most singular terms having been removed, equation (33) shows that the quantity $\partial\Psi^{(s)}/\partial Y$ remains constant as $Y \to \infty$. Thus, as

$$v_\mu^{(s)} = \frac{1}{c\left(1+\lambda_0^2\right)^{1/2}(1-\mu^2)^{1/2}}\frac{\partial\Psi^{(s)}}{\partial Y}$$

(which follows from (9), (14) and (17)), the tangential velocity field does not fade away at the outer edge of the Stokes layer ($Y \to \infty$). Rather, it yields a finite value which is seen from the main bulk of the fluid as the effective slip velocity on the body surface:

$$v^{(\mathrm{slip})} \equiv v_\mu^{(s)}\big|_{Y\to\infty} = \frac{A^2}{4c^3}\left[3\frac{\mu(1-\mu^2)^{3/2}}{\left(\lambda_0^2+\mu^2\right)^{5/2}} + 5\frac{\mu(1-\mu^2)^{1/2}}{\left(\lambda_0^2+\mu^2\right)^{3/2}}\right]. \quad (34)$$

https://doi.org/10.1017/S0022112003007122 Published online by Cambridge University Press

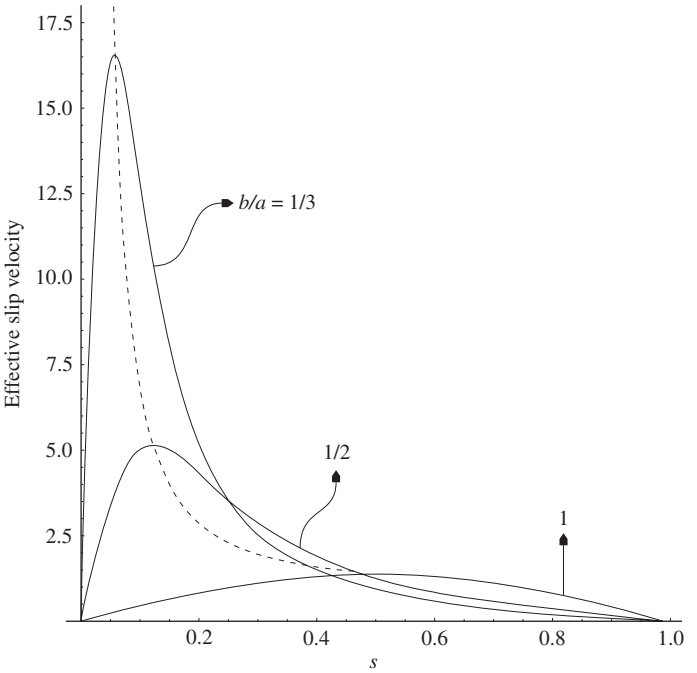


FIGURE 2. The effective slip velocity, equation (34), persisting at the outer edge of the Stokes layer as a function of the normalized distance along the surface, equation (36), for various aspect ratios. It is directed from the equator ($s = 0$) towards the pole ($s = 1$).

Applying the sphere limit (13) to (34) with (30), we recover the well-known result for the effective slip velocity on the surface of a sphere (see e.g. (5.18) in Yarin *et al.* 1999):

$$v^{(\mathrm{slip})} \equiv v_\mu^{(s)}\big|_{Y\to\infty} = \tfrac{45}{16}\mu\,(1-\mu^2)^{1/2} = \tfrac{45}{32}\sin 2\theta.$$

We note that the μ and θ velocity components are related by $v_\theta = -v_\mu$, and if the slip velocity is defined in terms of v_θ (rather than v_μ as here), a minus sign appears in the above formula.

Applying the matching principle (20) to the steady part of the flow and taking (17) and (33) into account, we deduce

$$\lambda = \lambda_0\colon \quad \psi^{(s)} = 0, \quad \frac{\partial \psi^{(s)}}{\partial \lambda} = \frac{A^2}{4c}\left[3\frac{\mu(1-\mu^2)^2}{\left(\lambda_0^2+\mu^2\right)^2} + 5\frac{\mu(1-\mu^2)}{\lambda_0^2+\mu^2}\right] \tag{35}$$

which serve as boundary conditions for the outer steady flow. While the displacement effect of the Stokes layer is negligible to leading order, which is expressed by the first condition (35), the effective slip velocity appearing in the second condition (35) is what drives steady streaming in the outer region.

The sign of (34) is such that the effective slip velocity is directed from the equator towards the poles. The distribution (34) is shown in figure 2 for various aspect ratios of the oblate spheroid. Rather than μ, it is more illustrative to use as a surface coordinate the distance along the surface, x (the arc length). Furthermore, we use the relative distance, s, for convenience in simultaneously representing results for different

https://doi.org/10.1017/S0022112003007122 Published online by Cambridge University Press

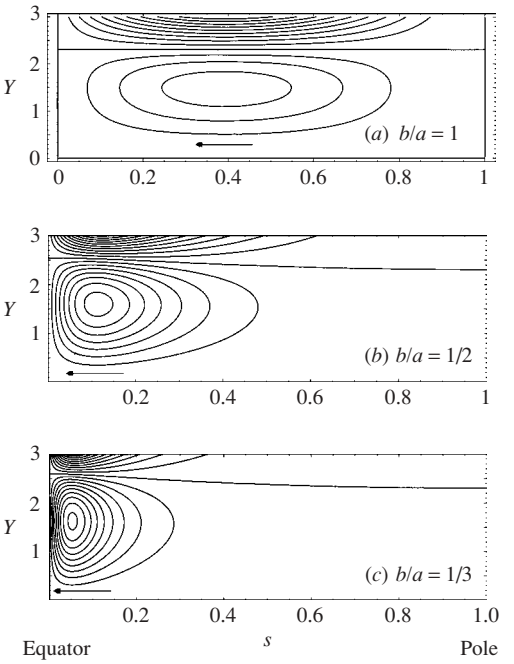


FIGURE 3. Steady streaming pattern in the Stokes layer at the surface of an oblate spheroid, equation (33), for various aspect ratios. The flow is shown in the domain formed by the normalized distance along the surface (horizontal) and the scaled distance from the surface (vertical). Here $s = 0$ corresponds to the equator and $s = 1$ to the pole of the spheroid. Vertical proportions are highly exaggerated. The arrows indicate direction of the flow. The streamlines are drawn at the intervals 0.03, 0.1 and 0.3 for the three cases shown, respectively.

aspect ratios. We have (cf. h_μ in Appendix A)

$$x(\mu) = \int_0^\mu \frac{c\left(\lambda_0^2 + \mu'^2\right)^{1/2}}{(1-\mu'^2)^{1/2}}\,\mathrm{d}\mu' = c\,\lambda_0\,\mathrm{Ei}\left(\arcsin\mu, -\frac{1}{\lambda_0^2}\right)$$
$$= c\,\left(1+\lambda_0^2\right)^{1/2}\left[\mathrm{Ei}\left(\frac{1}{1+\lambda_0^2}\right) - \mathrm{Ei}\left(\arccos\mu, \frac{1}{1+\lambda_0^2}\right)\right], \quad s(\mu) = \frac{x(\mu)}{x(1)}, \quad (36)$$

where $\mathrm{Ei}(\varphi, m)$ is the incomplete elliptic integral of the second kind, while $\mathrm{Ei}(m)$ is the complete elliptic integral of the second kind, m being the modulus. Here s varies in the limits $-1 \leqslant s \leqslant 1$ with $s = 0$ ($x = 0$) defined to be at the equator of the spheroid, while $s = \pm 1$ correspond to the poles. In view of the symmetry with respect to the equatorial plane, the distribution over only one hemisphere is shown in figure 2. For any given aspect ratio b/a, the parameter λ_0 is determined from (7), while c is as in (8).

The streamlines for the steady flow in the Stokes layer are represented in figure 3 according to equation (33). A thin boundary-layer zone along the curved surface is unfolded into a rectangular region, and the normal proportions are highly exaggerated. The relative distance along the surface, equation (36), is again used in the plot.

The results depicted in figures 2 and 3 show that the streaming intensity sharply increases on decreasing the aspect ratio b/a of the oblate spheroid, the other constraints being the same. Furthermore, it is not only that the intensity increases: the centre of the streaming (the location where the maximal intensity is achieved)

https://doi.org/10.1017/S0022112003007122 Published online by Cambridge University Press

becomes strongly displaced towards the sharp edge of the particle, i.e. towards the equatorial plane ($s=0$). In particular, the location of the slip velocity maximum is seen to approach $s=0$ as b/a is decreased. Such spikyness of the slip velocity distribution has also been observed in other streaming problems involving ellipses (Davidson & Riley 1972; Riley & Wybrow 1995). The streamlines become much denser around the sharp-edged equator than in other parts of the region. In other respects, the steady flow pattern in the Stokes layer is topologically similar to that of a sphere (the case shown in figure 3*a*), with a zone of recirculation covering the surface of the particle. However, unlike the sphere, the thickness of this zone becomes slightly non-uniform. A consequence of the recirculation is that the effective slip velocity at the outer edge of the Stokes layer and the tangential shear stress at the surface are in opposite directions.

Let us also mention that the effective slip velocity distribution obtained numerically by Yarin *et al.* (1999) for acoustically levitated drops and shown in their figure 14 is qualitatively similar to the present one: the streaming is directed to the poles, and a tendency towards the earlier mentioned spikyness of the distribution is observed in their figure 14(*a*), where the largest drop (presumably the most squeezed one) is considered. However, quantitative comparison is not possible here for lack of certain data.

It is of interest to discuss the asymptotic behaviour of the streaming characteristics as the aspect ratio tends to zero (the circular disk limit). For this purpose, we choose λ_0 as the small parameter, and establish the scalings for the variables $v_\mu^{(s)}$, x, s and μ in the zone of the most violent streaming, which are readily obtained by following the maximum of the effective slip velocity (34). For the geometric characteristics of the spheroid, from (6)–(8), we have

$$a=1, \quad b=\lambda_0+O\left(\lambda_0^3\right), \quad c=1+O\left(\lambda_0^2\right) \qquad \text{as} \quad \lambda_0\to 0.$$

From (34) and (36), we obtain, in the region of maximum streaming velocity,

$$v_\mu^{(s)}=O\left(\lambda_0^{-4}\right), \quad x=O\left(\lambda_0^2\right), \quad s=O\left(\lambda_0^2\right), \quad \mu=O(\lambda_0) \qquad \text{as} \quad \lambda_0\to 0. \tag{37}$$

Notice that the coordinate scalings in (37) characterize the extent of the violent-streaming zone around the equator $x=s=\mu=0$, and that the scalings (37) go along with the tendencies observed in figures 2 and 3 as the aspect ratio is decreased.

A further interpretation of this result is possible if we note that the dimensionless radius of curvature $\mathscr{R}_c$ (non-dimensionalized with l, which is here chosen to be the major radius of the spheroid) taken at the sharp-edged equator of the oblate spheroid is

$$\mathscr{R}_c=O\left(\lambda_0^2\right) \quad \text{as } \lambda_0\to 0. \tag{38}$$

Consequently, $x\propto\mathscr{R}_c$ ($s\propto\mathscr{R}_c$) as $\lambda_0\to 0$, i.e. the most intense streaming occurs on the scale of the equatorial radius of curvature. Next, we turn to interpreting the scaling for $v_\mu^{(s)}$. First, we note that in the absence of sharp edges, i.e. for $b/a=O(1)$ in the case of our spheroid, the order of magnitude of the steady velocity (in dimensional form) is

$$U_\infty\,\varepsilon=\frac{U_\infty^2}{\omega\, l}. \tag{39}$$

In the case $\lambda_0\ll 1$, the near-equator steady velocity is $O(\lambda_0^{-4})$ times higher:

$$\frac{U_\infty^2}{\omega\, l}\frac{1}{\lambda_0^4}\propto\frac{(U_\infty/\lambda_0)^2}{\omega\,(l\,\mathscr{R}_c)}=\frac{\tilde{U}_\infty^2}{\omega\tilde{l}}=\tilde{U}_\infty\,\tilde{\varepsilon} \tag{40}$$

https://doi.org/10.1017/S0022112003007122 Published online by Cambridge University Press

with

$$\tilde{U}_\infty = \frac{U_\infty}{\lambda_0}, \quad \tilde{l} = l\,\mathscr{R}_c, \quad \tilde{\varepsilon} = \frac{\tilde{U}_\infty}{\omega \tilde{l}} \propto \frac{\varepsilon}{\lambda_0^3},$$

where the terms have been regrouped so that the scaling pattern (39) is observed in the newly defined quantities with a tilde. Here $\tilde{l}$ is the appropriate length scale (of order of the radius of curvature) in the vicinity of the equator, while $\tilde{U}_\infty$ is the appropriate velocity scale of the primary oscillatory flow in the same vicinity. The latter can be seen from (9) and (26) by taking the limit $\lambda = \lambda_0 \to 0$ while $\mu = O(\lambda_0)$. Thus, the scalings (37) are consistent with the pattern (39), as expected.

Another way of establishing the scaling $\tilde{U}_\infty = U_\infty/\lambda_0$, without recourse to the results of § 3, is to refer to a planar flow with the complex potential $w(\xi) = C\,\xi^{1/2}$. It is expected to represent the behaviour of the primary oscillatory flow in a small vicinity of the edge of a disk-like body, over distances which are on the one hand much smaller than the principal radius of the body, and on the other hand much greater than the radius of curvature at the edge (the latter is not required in the case of an oblate spheroid, for if $\xi = 0$ is chosen to be in the focus of the spheroid the flow $w(\xi) = C\,\xi^{1/2}$ holds up to the surface to the leading order in λ_0). Then, if the velocity scale is $O(1)$ over distances $O(1)$ from the edge, it should be $O(\mathscr{R}_c^{-1/2})$ over distances $O(\mathscr{R}_c)$. Thus, in view of (38), we obtain that $\tilde{U}_\infty \propto U_\infty/\lambda_0$.

All the above arguments show that the asymptotic scaling (37) is applicable not only to oblate spheroids but also to arbitrary disk-like bodies with a smooth edge (i.e. when the radius of curvature varies smoothly over distances of the order of its size in the vicinity of the equator), provided that λ_0 is understood according to (38). For scaling purposes, we may choose $\lambda_0 = \mathscr{R}_c^{1/2}$. Thus, $v_\mu^{(s)} = O(\mathscr{R}_c^{-2})$ as $\mathscr{R}_c \to 0$. But, of course, a particular numerical factor hidden here depends on the body shape. Let us underscore once again that, concerning the order of magnitude of the steady streaming in the disk limit, the key parameter is the dimensionless radius of curvature at the edge, but not the aspect ratio. Two different smooth-edged disk-like bodies with the same order of magnitude of $\mathscr{R}_c$ are expected to produce streaming of the same order of magnitude. But this is generally not true for two bodies of the same aspect ratio b/a. Note that, regarding the relation between $\mathscr{R}_c$ and b/a, for the oblate spheroid we have $\mathscr{R}_c = O(b^2)$ as $b \to 0$ ($a = 1$), while ordinarily one would expect $\mathscr{R}_c = O(b)$, as e.g. for a disk with a rounded edge. In this sense, the oblate spheroid is not quite a typical representative of the above mentioned class of disk-like bodies: in the disk limit, its edge sharpens much faster than the aspect ratio decreases.

It is clear that in the disk limit the conditions (4) for small amplitude and high frequency should be reinforced. It is now the radius of curvature at the edge in comparison to which both the amplitude of fluid particle displacement and the Stokes layer thickness should be small. This leads to

$$\tilde{\varepsilon} \propto \frac{\varepsilon}{\lambda_0^3} \ll 1, \qquad \tilde{M}^2 = \frac{\omega \tilde{l}^2}{\nu} \propto M^2\,\lambda_0^4 \gg 1, \tag{41}$$

which are more restrictive conditions than (4). The newly defined small parameter $\tilde{\varepsilon}$ ensures there will be no flow separation from the, increasingly sharp, edge.

5. Problem formulation for outer streaming

Now we return to the main bulk of the fluid (i.e. outside the Stokes layer) and consider steady streaming therein (the outer streaming). Using (21) in (10), and taking

https://doi.org/10.1017/S0022112003007122 Published online by Cambridge University Press

the time-average, we arrive at

$$\varepsilon\langle \mathrm{N}(\psi^{(u)}, \mathrm{E}^2\psi^{(u)})\rangle + \varepsilon^3 \mathrm{N}(\psi^{(s)}, \mathrm{E}^2\psi^{(s)}) = \frac{\varepsilon}{M^2}\mathrm{E}^4\psi^{(s)}. \tag{42}$$

To leading order, the fluctuating part of the flow is irrotational, with $\mathrm{E}^2\psi^{(u)} = 0$, and the first term on the left-hand side of (42) vanishes. This corresponds to the fact that the steady streaming is not forced in the main bulk of the fluid, but rather in the Stokes layer. Nevertheless, the term in question may yet yield a higher-order contribution important in (42). It is clear that such a contribution can come only from a *rotational* part in $\psi^{(u)}$.

To further explore this point, we derive an equation for $\psi^{(u)}$ by subtracting (42) from (10) while keeping (21) in mind. We obtain

$$\frac{\partial \mathrm{E}^2\psi^{(u)}}{\partial t} + \varepsilon\big[\mathrm{N}(\psi^{(u)}, \mathrm{E}^2\psi^{(u)}) - \langle \mathrm{N}(\psi^{(u)}, \mathrm{E}^2\psi^{(u)})\rangle + \varepsilon \mathrm{N}(\psi^{(s)}, \mathrm{E}^2\psi^{(u)}) + \varepsilon \mathrm{N}(\psi^{(u)}, \mathrm{E}^2\psi^{(s)})\big] = \frac{1}{M^2}\mathrm{E}^4\psi^{(u)}. \tag{43}$$

From (43), we observe that the only way a rotational part can arise in $\psi^{(u)}$ is through a nonlinear interaction with the steady component of the flow. In the same manner as (21), we write

$$\psi^{(u)} = \psi^{(u/p)} + \varepsilon^2\psi^{(u/r)}, \tag{44}$$

separating the fluctuating component of the flow into potential and rotational parts, $\psi^{(u/p)}$ and $\psi^{(u/r)}$, respectively. The asymptotic order of the latter, $O(\varepsilon^2)$, is deduced from equation (43). With (44), the first term in (42) becomes

$$\varepsilon^3\langle \mathrm{N}(\psi^{(u/p)}, \mathrm{E}^2\psi^{(u/r)})\rangle \tag{45}$$

which is, remarkably, of the same order as the second term.

Using (44) in (43), we arrive at the following leading-order equation for the rotational part:

$$\frac{\partial \mathrm{E}^2\psi^{(u/r)}}{\partial t} + N\left(\psi^{(u/p)}, \mathrm{E}^2\psi^{(s)}\right) = 0.$$

With $\psi^{(u/p)}$ given by (26), we obtain

$$\mathrm{E}^2\psi^{(u/r)} = \mathrm{i}\,\mathrm{N}(\psi^{(u/p)}, \mathrm{E}^2\psi^{(s)}) \tag{46}$$

which should be substituted into (45). Now phase differences come into play. In the present problem, the leading-order oscillation (26) has a single phase. Consequently, as seen from (46), $\mathrm{E}^2\psi^{(u/r)}$ is out of phase with $\psi^{(u/p)}$ (i.e. the phase difference is $\pi/2$), and after taking the time average, the term (45), and thus the first term on the left-hand side of (42), vanishes. Therefore, to leading order, equation (42) becomes just the ordinary steady Navier–Stokes equation:

$$\mathrm{N}(\psi^{(s)}, \mathrm{E}^2\psi^{(s)}) = \frac{1}{R_s}\mathrm{E}^4\psi^{(s)} \tag{47}$$

where the notation

$$R_s = \varepsilon^2 M^2 = \frac{U_\infty^2}{\omega\nu} \tag{48}$$

has been introduced following Riley (1966, 1967). As is evident from equation (47), R_s plays the role of the streaming Reynolds number. It is a product of a small and a large parameter, and can in principle take any value, from small to large.

https://doi.org/10.1017/S0022112003007122 Published online by Cambridge University Press

A situation where the leading-order oscillatory flow is not in phase and an additional term arises in the steady Navier–Stokes equation is pointed out by Riley (2001).

Another consequence of the primary oscillatory flow having a single phase is that the Eulerian flow, represented by $\psi^{(s)}$, is not different from the Lagrangian mean flow (for the definition of the latter see e.g. Nyborg (1965) and Riley (2001)). Similarly, the mean flow in the reference frame where the particle is at rest is the same as in the reference frame where the medium at infinity is at rest. And the same is true for any reference frame which oscillates in phase with our primary oscillatory flow. The latter remark is of relevance to the situation when the particle is freely suspended in an oscillating fluid of comparable density. In this case, the particle is also set into oscillatory motion, whose amplitude is comparable to that in the fluid medium far away from it. However, to leading order, these oscillations are in phase. Therefore, the steady flow in the laboratory frame of reference is not different from the one considered here. Thus, to leading order, the outer mean flows in all the above senses are identical here, and are all represented by $\psi^{(s)}$, the problem statement for which is elaborated in the present section.

With equation (47) and the boundary conditions (35) derived earlier, the problem formulation for the steady streaming in the main bulk of the fluid is completed by requiring the steady flow to fade away far from the spheroid:

$$\lambda \to \infty: \quad \psi^{(s)}/\lambda^2 \to 0. \tag{49}$$

Thus, the problem for the outer streaming is given by (35), (47) and (49). It is solved in the following two sections in the limits of small and large streaming Reynolds number, respectively.

Finally, let us point out what can be expected for the outer streaming in the limit of a spheroid with small aspect ratio ($\lambda_0 \to 0$). Following the developments in the Stokes layer, discussed at the end of § 4, a localized steady streaming of high intensity is expected to extend into the outer region around the sharp-edged equator. In view of (37), the velocity scales as $O(\lambda_0^{-4})$, while the spatial scale is of the order of the radius of curvature at the equator, i.e. $O(\lambda_0^{-2})$. Then the appropriate streaming Reynolds number for this localized violent flow is

$$\tilde{R}_s = \tilde{\varepsilon}^2 \tilde{M}^2 = \frac{\tilde{U}_\infty^2}{\omega \nu} = \frac{R_s}{\lambda_0^2} \tag{50}$$

which is asymptotically higher than R_s defined in (48). As we shall see, the streaming intensity in the main part of the outer region is determined by the speed of the natural decay away from the tiny zone of violent streaming. The effective slip velocity will be found to be decreasing too fast away from the equator and accordingly loses its influence upon the streaming.

To develop a consistent asymptotic approach to the outer streaming in the limit $\lambda_0 \to 0$, one has to consider the solution separately in two zones with subsequent matching. The first zone is the small one in the vicinity of the equator where the streaming is the most violent, while the second zone is the rest of the outer region. Such an approach is easily realizable and especially effective in the case of large streaming Reynolds numbers, and is carried out in § 8.

6. Outer streaming in the Stokes approximation

In the present section, we consider the problem of steady streaming in the main bulk of the fluid around the oblate spheroid, and treat it in the limit $R_s \ll 1$. In this

https://doi.org/10.1017/S0022112003007122 Published online by Cambridge University Press

limit, equation (47) becomes the Stokes equation

$$\mathrm{E}^4\psi^{(s)} = 0 \tag{51}$$

while the boundary conditions are still given by (35) and (49).

We look for a solution of the Stokes equation $\mathrm{E}^4\psi = 0$ by making use of the fact that (Neuber–Papkovich formulation)

$$\psi = \psi_1^{(p)} + \lambda\mu\psi_2^{(p)} \tag{52}$$

is a solution of the Stokes equation $\mathrm{E}^4\psi = 0$ provided that $\psi_1^{(p)}$ and $\psi_2^{(p)}$ are solutions of the potential flow equation $\mathrm{E}^2\psi = 0$, which can be easily verified by direct substitution. This will prove sufficient for constructing the solution of our problem.

To obtain a potential-flow solution, we write $\psi^{(p)} = X(\lambda)Y(\mu)$. Upon substitution into $\mathrm{E}^2\psi^{(p)} = 0$, the variables are separated, and we arrive at

$$\frac{1+\lambda^2}{X}\frac{\mathrm{d}^2X}{\mathrm{d}\lambda^2} = -\frac{1-\mu^2}{Y}\frac{\mathrm{d}^2Y}{\mathrm{d}\mu^2} = n(n-1) \tag{53}$$

where the constant has been written as $n(n-1)$. The resulting equation for $Y(\mu)$ is the same as in the spherical case (Happel & Brenner 1965), and only non-negative integer values of n are to be considered. For a given n, two independent solutions of equation (53) for $Y(\mu)$ are $G_n(\mu)$ and $H_n(\mu)$, which are the Gegenbauer functions of the first and second kinds, respectively, order n and degree $-1/2$. These functions are related in a simple way to the more familiar Legendre functions $P_n(\mu)$ and $Q_n(\mu)$, respectively of the first and second kinds, by

$$G_n(\mu) = \frac{P_{n-2}(\mu) - P_n(\mu)}{2n-1}, \quad H_n(\mu) = \frac{Q_{n-2}(\mu) - Q_n(\mu)}{2n-1} \quad \text{for } n \geqslant 2, \tag{54}$$

while for $n = 0, 1$ they are defined as

$$G_0(\mu) = 1, \quad G_1(\mu) = -\mu, \quad H_0(\mu) = -\mu, \quad H_1(\mu) = -1. \tag{55}$$

Some other of the functions are

$$G_2(\mu) = \tfrac{1}{2}(1-\mu^2), \quad G_3(\mu) = \tfrac{1}{2}\mu(1-\mu^2), \quad H_2(\mu) = \tfrac{1}{4}(1-\mu^2)\ln\left(\frac{1+\mu}{1-\mu}\right) + \tfrac{1}{2}\mu.$$

The properties of the Gegenbauer functions here are cited from Happel & Brenner (1965), who in turn make reference to Sampson (1891).

When considering a complex variable ξ, single-valued branches of $H_n(\xi)$, as well as of $Q_n(\xi)$, are defined in the complex plane cut along the interval $[-1, 1]$ of the real axis. The branch that yields real values on the real axis outside the cut is selected. The values on the real interval $-1 < \mu < 1$ are then defined by the average of the values at the upper and lower edges of the cut, i.e. $H_n(\mu) \equiv [H_n(\mu + \mathrm{i}0) + H_n(\mu - \mathrm{i}0)]/2$. Relations (54) and expressions for the functions formally remain the same in terms of a complex variable ξ, except for the logarithmic terms, which undergo a sign change under the logarithm, e.g.

$$H_2(\xi) = \tfrac{1}{4}(1-\xi^2)\ln\left(\frac{1+\xi}{\xi-1}\right) + \tfrac{1}{2}\xi.$$

Now two independent solutions of equation (53) for $X(\lambda)$ can be written as $G_n(\mathrm{i}\lambda)$ and $H_n(\mathrm{i}\lambda)$. For convenience, we define the following 'modified' Gegenbauer functions:

$$\tilde{G}_n(\lambda) = (-1)^{n-1}\mathrm{i}^n G_n(\mathrm{i}\lambda), \qquad \tilde{H}_n(\lambda) = (-1)^{n-1}\mathrm{i}^{n+1} H_n(\mathrm{i}\lambda), \tag{56}$$

https://doi.org/10.1017/S0022112003007122 Published online by Cambridge University Press

which are all real within the present study. It turns out that $\tilde{G}_n(\lambda) = O(\lambda^n)$, $\tilde{H}_n(\lambda) = O(\lambda^{1-n})$ as $\lambda \to +\infty$. Some lowest-order functions are

$$\tilde{G}_0(\lambda) = -1,\ \tilde{G}_1(\lambda) = \lambda,\ \tilde{G}_2(\lambda) = \tfrac{1}{2}(1+\lambda^2), \tilde{G}_3(\lambda) = \tfrac{1}{2}\lambda(1+\lambda^2),\ \tilde{H}_0(\lambda) = -\lambda,$$
$$\tilde{H}_1(\lambda) = 1,\ \tilde{H}_2(\lambda) = \tfrac{1}{2}(1+\lambda^2)\mathrm{arccot}\lambda - \tfrac{1}{2}\lambda,\ \tilde{H}_3(\lambda) = \tfrac{1}{2}\lambda(1+\lambda^2)\mathrm{arccot}\lambda - \tfrac{1}{2}\lambda^2 - \tfrac{1}{3}. \quad (57)$$

Explicit expressions for all the functions that will be needed here have been cited for reference in Appendix B.

The required potential-flow solutions can now be written as

$$\left.\begin{aligned} \psi_1^{(p)} &= \sum_{n=0}^{\infty} [a_n \tilde{G}_n(\lambda) + c_n \tilde{H}_n(\lambda)] G_n(\mu), \\ \psi_2^{(p)} &= \sum_{n=1}^{\infty} [b_n \tilde{G}_{n-1}(\lambda) + d_n \tilde{H}_{n-1}(\lambda)] G_{n-1}(\mu), \end{aligned}\right\} \quad (58)$$

where a_n, b_n, c_n and d_n are arbitrary constants. The numeration in the second expression is adjusted in anticipation of a convenient manipulation in (52). Solutions similar to (58) can be written by using $H_n(\mu)$ instead of $G_n(\mu)$. However, they are discarded, as the terms with $H_0(\mu)$ and $H_1(\mu)$ would be redundant, while the terms with $H_n(\mu)$ ($n \geqslant 2$) would lead to singularities in the velocity field as $\mu \to \pm 1$, which is unacceptable here. Actually, some of the terms with $G_0(\mu)$ and $G_1(\mu)$ also lead to such singularities. They are kept for manipulations in (52), and what remains of them is disregarded later.

Using the identity (Happel & Brenner 1965)

$$\mu G_{n-1}(\mu) = \frac{n}{2n-3} G_n(\mu) + \frac{n-3}{2n-3} G_{n-2}(\mu) \quad (59)$$

valid for $n \geqslant 2$, as well as $\mu G_0(\mu) = -G_1(\mu)$, we obtain

$$\begin{aligned} \lambda\mu\psi_2^{(p)} = &-\lambda[b_2\tilde{G}_1(\lambda) + d_2\tilde{H}_1(\lambda)]G_0(\mu) - \lambda[b_1\tilde{G}_0(\lambda) + d_1\tilde{H}_0(\lambda)]G_1(\mu) \\ &+ \lambda \sum_{n=2}^{\infty} \left[(b_n\tilde{G}_{n-1}(\lambda) + d_n\tilde{H}_{n-1}(\lambda)) \frac{n}{2n-3} \right. \\ &\left. + (b_{n+2}\tilde{G}_{n+1}(\lambda) + d_{n+2}\tilde{H}_{n+1}(\lambda)) \frac{n-1}{2n+1} \right] G_n(\mu). \end{aligned} \quad (60)$$

Now we substitute (58) and (60) into (52), and cancel out the terms that result in singularities for the velocity field. As seen from (9), those are the λ-dependent terms at $G_0(\mu)$ and $G_1(\mu)$. We find

$$c_0 + d_2 = 0, \quad b_2 = 0, \quad a_1 + b_1 = 0, \quad d_1 = 0, \quad (61)$$

while a_0 and c_1 remain free. A noteworthy result here is that the coefficient b_2, which also appears at the mode $G_2(\mu)$, should vanish, while no limitations are imposed on d_2.

The counterpart of (59) for the modified Gegenbauer functions,

$$\lambda\{\tilde{G}_n(\lambda),\ \tilde{H}_n(\lambda)\} = \frac{n+1}{2n-1}\{\tilde{G}_{n+1}(\lambda),\ \tilde{H}_{n+1}(\lambda)\} - \frac{n-2}{2n-1}\{\tilde{G}_{n-1}(\lambda),\ \tilde{H}_{n-1}(\lambda)\}, \quad (62)$$

is used to further transform (60). Notice that (62) holds for $\tilde{G}_n(\lambda)$ at $n \geqslant 1$, while for $\tilde{H}_n(\lambda)$ it is valid only at $n \geqslant 3$. Hence, for $n = 1$ and $n = 2$ we use $\lambda\tilde{H}_1(\lambda) = -\tilde{H}_0(\lambda)$ and $\lambda\tilde{H}_2(\lambda) = \tilde{H}_3(\lambda) + \tilde{H}_1(\lambda)/3$ obtained from (57). Using these identities and (61)

https://doi.org/10.1017/S0022112003007122 Published online by Cambridge University Press

upon substitution of (58) and (60) into (52), and redefining the free coefficients to obtain as simple an expression as possible, we arrive at

$$\psi = a_0 G_0(\mu) + c_1 G_1(\mu) + \sum_{n=4}^{\infty} b_n \tilde{G}_{n-2}(\lambda)\, G_n(\mu)$$
$$+ \sum_{n=2}^{\infty} [a_n \tilde{G}_n(\lambda) + c_n \tilde{H}_n(\lambda) + d_n \tilde{H}_{n-2}(\lambda) - b_{n+2}\tilde{G}_{n+2}(\lambda) - d_{n+2}\tilde{H}_{n+2}(\lambda)] G_n(\mu) \quad (63)$$

which is the most general form of the solution of the Stokes equation that we have been able to obtain and that does not imply singularities for the velocity field at the symmetry axis.

A remarkable feature of (63) is an apparent asymmetry that emerges between the functions $\tilde{G}_n(\lambda)$ and $\tilde{H}_n(\lambda)$. Namely, we effectively have $b_2 \equiv 0$ and $b_3 \equiv 0$, while their counterparts d_2 and d_3 are present. For b_2, this occurred in (61); b_3 was effectively absorbed into a_3, whereas d_3 remained present owing to (62) not holding at $n = 2$ for functions of the second kind. Thus, application of (63) to the exterior and interior problems is procedurally not quite identical. Note that by taking the limit $\lambda \to \infty$ in (63), the corresponding solution in the spherical coordinates (see Happel & Brenner 1965) is fully recovered.

Now we move closer to the problem (35), (49) and (51). The only inhomogeneity, occurring in (35), can be expanded as a series in $G_n(\mu)$. Thus, we first solve the following auxiliary problem:

$$\left.\begin{array}{l} \mathrm{E}^4 \psi_n = 0, \\ \lambda \to \infty: \quad \psi_n/\lambda^2 \to 0, \quad \lambda = \lambda_0: \quad \psi_n = 0, \ \partial\psi_n/\partial\lambda = G_n(\mu) \end{array}\right\} \quad (64)$$

with $n \geqslant 2$. We make use of (63). From the condition as $\lambda \to \infty$, it is immediately obvious that $a_n = 0$ ($n \geqslant 2$) and $b_n = 0$ ($n \geqslant 4$). Also, the first two terms of (63) contradict the non-penetration condition at the surface of the spheroid, hence $a_0 = c_1 = 0$. After inspecting the remaining terms in (63), it is clear that the solution of (64) can be sought in the form of a finite series

$$\psi_n = {\sum_{k=[n]}^{n}}' \left[c_k^{(n)} \tilde{H}_k(\lambda) + d_k^{(n)} \tilde{H}_{k-2}(\lambda)\right] G_k(\mu) - {\sum_{k=[n]}^{n-2}}' d_{k+2}^{(n)} \tilde{H}_{k+2}(\lambda)\, G_k(\mu) \quad (65)$$

where $[n] = 2$ if n is an even number, and $[n] = 3$ if n is odd. The prime at the summation symbol indicates that the summation is carried out with step equal to 2. If the lower limit exceeds the upper one, the sum equals to zero by convention. We just note that for the interior counterpart of the exterior problem (64), one would have to resort to an infinite series.

Using (65) in the boundary conditions (64) at $\lambda = \lambda_0$, one obtains the following system of equations for the coefficients:

$$c_n^{(n)} \tilde{H}_n(\lambda_0) + d_n^{(n)} \tilde{H}_{n-2}(\lambda_0) = 0,$$
$$c_n^{(n)} \frac{\mathrm{d}\tilde{H}_n}{\mathrm{d}\lambda}(\lambda_0) + d_n^{(n)} \frac{\mathrm{d}\tilde{H}_{n-2}}{\mathrm{d}\lambda}(\lambda_0) = 1,$$
$$c_k^{(n)} \tilde{H}_k(\lambda_0) + d_k^{(n)} \tilde{H}_{k-2}(\lambda_0) - d_{k+2}^{(n)} \tilde{H}_{k+2}(\lambda_0) = 0,$$
$$c_k^{(n)} \frac{\mathrm{d}\tilde{H}_k}{\mathrm{d}\lambda}(\lambda_0) + d_k^{(n)} \frac{\mathrm{d}\tilde{H}_{k-2}}{\mathrm{d}\lambda}(\lambda_0) - d_{k+2}^{(n)} \frac{\mathrm{d}\tilde{H}_{k+2}}{\mathrm{d}\lambda}(\lambda_0) = 0,$$

https://doi.org/10.1017/S0022112003007122 Published online by Cambridge University Press

where $k = [n], [n]+2, \ldots, n-4, n-2$. The solution is

$$\left.\begin{aligned} c_k^{(n)} &= -(-1)^{(n-k)/2}\frac{\tilde{H}_n(\lambda_0)\ \mathrm{W}[\tilde{H}_{k+2}(\lambda),\tilde{H}_{k-2}(\lambda)]\big|_{\lambda=\lambda_0}}{\mathrm{W}[\tilde{H}_k(\lambda),\tilde{H}_{k-2}(\lambda)]\big|_{\lambda=\lambda_0}\mathrm{W}[\tilde{H}_{k+2}(\lambda),\tilde{H}_k(\lambda)]\big|_{\lambda=\lambda_0}} \quad (\text{for } k<n),\\ c_n^{(n)} &= -\frac{\tilde{H}_{n-2}(\lambda_0)}{\mathrm{W}[\tilde{H}_n(\lambda),\tilde{H}_{n-2}(\lambda)]\big|_{\lambda=\lambda_0}}, \quad d_k^{(n)} = (-1)^{(n-k)/2}\frac{\tilde{H}_n(\lambda_0)}{\mathrm{W}[\tilde{H}_k(\lambda),\tilde{H}_{k-2}(\lambda)]\big|_{\lambda=\lambda_0}}, \end{aligned}\right\} \tag{66}$$

with the operator W defined as

$$\mathrm{W}[f(\lambda),g(\lambda)] = f\frac{\mathrm{d}g}{\mathrm{d}\lambda} - \frac{\mathrm{d}f}{\mathrm{d}\lambda}g$$

where $f(\lambda)$ and $g(\lambda)$ are arbitrary functions.

Thus, the solution of (64) is determined by (65), (66).

Now we are ready to write down the solution of the problem (35), (49), (51). Representing the second condition (35) in the form

$$\lambda = \lambda_0: \quad \frac{\partial\psi^{(s)}}{\partial\lambda} = \sum_{n=2}^{\infty} q_n\, G_n(\mu) \tag{67}$$

the solution is

$$\psi^{(s)} = \sum_{n=2}^{\infty} q_n\, \psi_n. \tag{68}$$

The coefficients q_n are found to be

$$q_n = \frac{A^2}{4c}n(n-1)(2n-1)\left[1+(-1)^{n-1}\right]\mathrm{i}^{n-1}\left[\tilde{H}_n(\lambda_0) - \frac{3}{4}\frac{1+\lambda_0^2}{\lambda_0}\frac{\mathrm{d}\tilde{H}_n}{\mathrm{d}\lambda}(\lambda_0)\right] \tag{69}$$

(see Appendix C for details), where A is defined in (30). In view of the symmetry with respect to the equatorial plane of the spheroid, $q_n = 0$ for the even values of n.

Thus, the steady streaming in the main bulk of the fluid around an oblate spheroid is determined by (65), (66), (68) and (69). In view of (65) and (68), the solution actually involves a double series. By inverting the order of summation, the solution can also be rewritten in the form

$$\psi^{(s)} = {\sum_{k=3}^{\infty}}'[c_k\tilde{H}_k(\lambda) + d_k\tilde{H}_{k-2}(\lambda) - d_{k+2}\tilde{H}_{k+2}(\lambda)]G_k(\mu) \tag{70}$$

with

$$c_k = {\sum_{n=k}^{\infty}}' q_n c_k^{(n)}, \quad d_k = {\sum_{n=k}^{\infty}}' q_n d_k^{(n)}. \tag{71}$$

The streamlines for the steady flow around an oblate spheroid are shown in figure 4 for various aspect ratios. Just as happens in the Stokes layer, the flow pattern again appears to be topologically similar to that of a sphere, the flow intensity is drastically increased with the decrease of the aspect ratio b/a, and the streamlines tend to concentrate near the sharp-edged equator of the oblate spheroid.

From the viewpoint of processes in acoustic levitators, the streaming pattern studied here represents just microstreaming from a levitated particle, whereas in acoustic levitators there also exists streaming associated with the levitator as a whole which

https://doi.org/10.1017/S0022112003007122 Published online by Cambridge University Press

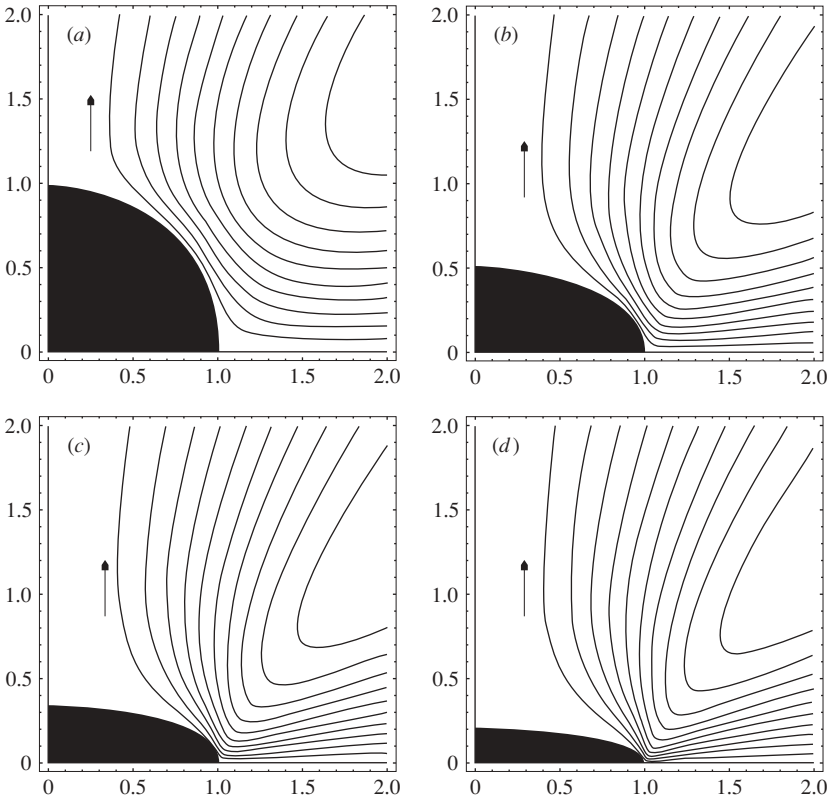


FIGURE 4. The outer streaming in the Stokes approximation, equation (70) with (66), (69) and (71), for various aspect ratios: (*a*) $b/a = 1$ (a sphere), (*b*) $b/a = 1/2$, (*c*) $b/a = 1/3$, and (*d*) $b/a = 1/5$. In view of the symmetry with respect to both the axis (vertical) and the equatorial plane (horizontal), only one quadrant of the flow pattern is displayed. The arrows indicate direction of the flow. The streamlines are drawn at the intervals 0.0416, 0.0816, 0.150 and 0.400 for the above four cases, respectively.

is superimposed on the microstreaming (Trinh & Robey 1994). Many observed streaming patterns in the vicinity of levitated particles are explained well by such superimposition, as confirmed by Rednikov & Riley (2002). On the other hand, as the microstreaming from the oblate spheroid is qualitatively similar to that from a sphere, we cannot expect that oblateness of a particle, as such, can account for the cases when observed streaming patterns differ from the simplest one (Trinh & Robey 1994).

7. Outer streaming at large Reynolds number

When the streaming Reynolds number, defined in (48), is large ($R_s \gg 1$), the outer streaming flow attains a boundary-layer structure over the surface of the spheroid with thickness $O(R_s^{-1/2})$. In view of (4) and (48), it is always much greater than the Stokes layer thickness, $O(1/M)$. Interestingly, the outer boundary layer can be viewed as a second flow structure appearing over the body surface, the first one being the Stokes layer (Stuart 1966).

In the present section, we use the boundary-layer approximation to analyse the outer streaming for $R_s \gg 1$. Such an analysis is more convenient in terms of the

https://doi.org/10.1017/S0022112003007122 Published online by Cambridge University Press

velocity components rather than the stream function. Furthermore, it is convenient to use the normal distance to the surface as a coordinate in lieu of $\lambda - \lambda_0$, and the corresponding normal velocity component instead of the λ-component. Focusing on the leading-order boundary-layer results, we write

$$y = R_s^{1/2} \frac{c\left(\lambda_0^2 + \mu^2\right)^{1/2}}{\left(1+\lambda_0^2\right)^{1/2}}(\lambda - \lambda_0), \quad v_\mu^{(s)} = \frac{R_s^{1/2}}{\varrho_0}\frac{\partial \psi^{(s)}}{\partial y}, \quad v_y^{(s)} = -\frac{R_s^{1/2}}{\varrho_0 h_{\mu 0}}\left(\frac{\partial \psi^{(s)}}{\partial \mu}\right)_y \tag{72}$$

and the problem (35), (47) and (49) can be reduced to

$$\frac{1}{\varrho_0 h_{\mu 0}}\frac{\partial}{\partial \mu}\left(\varrho_0 v_\mu^{(s)}\right) + \frac{\partial v_y^{(s)}}{\partial y} = 0, \tag{73}$$

$$\frac{v_\mu^{(s)}}{h_{\mu 0}}\frac{\partial v_\mu^{(s)}}{\partial \mu} + v_y^{(s)}\frac{\partial v_\mu^{(s)}}{\partial y} = \frac{\partial^2 v_\mu^{(s)}}{\partial y^2}, \tag{74}$$

$$y \to \infty: \quad v_\mu^{(s)} \to 0, \tag{75}$$

$$y = 0: \quad v_\mu^{(s)} = v^{(\mathrm{slip})}(\mu), \quad v_y^{(s)} = 0, \tag{76}$$

where the effective slip velocity is given by (34) with (30). The quantities ϱ_0 and $h_{\mu 0}$ are the distance from the symmetry axis, ϱ, and the metric coefficient, h_μ, taken at the surface of our oblate spheroid, $\lambda = \lambda_0$. Namely,

$$\varrho_0 = c\left(1+\lambda_0^2\right)^{1/2}(1-\mu^2)^{1/2}, \quad h_{\mu 0} = \frac{c\left(\lambda_0^2+\mu^2\right)^{1/2}}{(1-\mu^2)^{1/2}}.$$

As in the boundary layer we have $\psi^{(s)} = O(R_s^{-1/2})$ and $\lambda - \lambda_0 = O(R_s^{-1/2})$, all the variables appearing in (73)–(76) are $O(1)$. Equations (73) and (74) are the leading-order boundary-layer equations with axial symmetry (Schlichting 1979) with the pressure term equal to zero as the flow outside the boundary layer is of asymptotically smaller order of magnitude here. Equation (74) is deduced from equation (47) by following the same steps as described in § 2.3 with regard to the Stokes layer, setting the counterpart of Π to zero and using the definitions (72). The continuity equation (73) can be restored by equating $\partial^2\psi^{(s)}/\partial\mu\partial y$ as calculated from the second and third equalities in (72). Notice that equations (73) and (74) would look neater in terms of the variable x (distance along the surface), introduced in (36), since $\partial/\partial x = h_{\mu 0}^{-1}\,\partial/\partial\mu$. However, as the effective slip velocity is given explicitly as a function of μ, we will keep working in terms of μ.

As dictated by the direction of the effective slip velocity, convection in the boundary layer proceeds along the surface from the equatorial plane ($\mu = 0$) symmetrically towards the poles ($\mu = \pm 1$). The solution of (73)–(76) in the vicinity of $\mu = 0$ can be obtained by expanding the unknown functions in powers of μ. The coefficients of the expansion are functions of y only, and in this way one obtains a set of boundary-value problems for ordinary differential equations associated with each order of the expansion. Solution for the leading order can be found analytically, and corresponds to

$$v_\mu^{(s)} = c\,\lambda_0\,B^2\,\exp(-By)\,\mu + O(\mu^3), \qquad v_y^{(s)} = -B\,[1-\exp(-By)] + O(\mu^2), \tag{77}$$

with

$$B = \frac{A\sqrt{3+5\lambda_0^2}}{2c^2\lambda_0^3}.$$

https://doi.org/10.1017/S0022112003007122 Published online by Cambridge University Press

It is useful to notice that $B = 3\sqrt{5}/4$ in the sphere limit (13), while $B = \sqrt{3}/(\pi c \lambda_0^3)$ in the disk limit $\lambda_0 \to 0$.

Over the whole interval $-1 < \mu < 1$, the solution is found numerically. Due to the symmetry, it suffices to consider flow only over one half of the spheroid, say, $0 < \mu < 1$. A stepwise procedure similar to Davidson (1973) and Gopinath & Mills (1993) is used. It starts from $\mu = 0$ and goes downstream towards $\mu = 1$. The boundary-layer solution is found to proceed smoothly, without singularities, up to $\mu = 1$ for any aspect ratio of the oblate spheroid. However, a singularity occurs precisely at the pole, $\mu = 1$, where flow from the entire corresponding half of the spheroid self-collides. The singularity appears to be of geometrical nature, for it does not occur in the analogous problem of streaming over a cylinder (Riley 1975) where the collision is along a line, not at a point as here. As it is pertinent to a close vicinity of the symmetry axis and in this sense independent of the global shape of the body, the qualitative asymptotic understanding of the singularity attained by Amin & Riley (1990) carries over to the present case, and some details will be discussed below. Upon the self-collision at the pole, the boundary-layer flow erupts into a thin round jet along the symmetry axis, emanating from the pole. Asymptotic scaling for the jet will also be discussed later on.

Consider the mass and momentum fluxes in the boundary layer defined, respectively, as

$$j_{\mathrm{mass}}(\mu) \equiv 2\pi\varrho_0 \int_0^\infty v_\mu^{(s)} \mathrm{d}y = -2\pi \int_0^\mu \varrho_0(\mu')\, h_{\mu 0}(\mu')\, v_y^{(s)}(\mu', \infty)\, \mathrm{d}\mu', \tag{78}$$

$$j_{\mathrm{mom}}(\mu) \equiv 2\pi\varrho_0 \int_0^\infty \left(v_\mu^{(s)}\right)^2 \mathrm{d}y = -2\pi \int_0^\mu \varrho_0(\mu')\, h_{\mu 0}(\mu')\, \frac{\partial v_\mu^{(s)}}{\partial y}(\mu', 0)\, \mathrm{d}\mu', \tag{79}$$

where the alternative expressions in (78) and (79) follow from our boundary-layer formulation when rewritten in the integral form. The quantity $-v_y^{(s)}(\mu, \infty)$ corresponds to $y = \infty$ (outer edge of the boundary layer) and is the entrainment velocity into the boundary layer, whilst $-\partial v_\mu^{(s)}/\partial y$ is taken at $y = 0$ and represents the tangential stress whose action is formally responsible for the momentum flux variation along the boundary layer.

A direct numerical computation shows that both j_{mass} and j_{mom} remain finite when approaching the pole, $\mu \to 1$, which also seems intuitively right. Working in an asymptotically small vicinity of the pole in order to clear up the nature of the singularity, let $(1 - \mu) \equiv \delta^2 \ll 1$ be the small parameter, which also corresponds to $(x(1) - x) = O(\delta)$, or $(1 - s) = O(\delta)$ in terms of the distance along the surface (36). With $\varrho_0 = O(\delta)$, $j_{\mathrm{mass}} = O(1)$ and $j_{\mathrm{mom}} = O(1)$, equations (78) and (79) leave no other possibility than $v_\mu^{(s)} = O(1)$, $y = O(\delta^{-1})$ as $\delta \to 0$. Consequently, the tangential velocity remains finite, while $y = O(\delta^{-1})$ means that the boundary-layer thickness drastically increases, as $O(\delta^{-1})$, when approaching the pole. With such a large thickness, the boundary layer becomes effectively inviscid, as can be established with the help of equation (74). However, as elaborated by Amin & Riley (1990), also present is a much thinner sublayer where viscous effects are important. Regarding the normal velocity, the continuity equation (73) yields $v_y^{(s)} = O(\delta^{-2})$, i.e. an even more drastic increase as $\delta \to 0$ than for the thickness.

Some representative numerical results for the boundary-layer flow are shown in figures 5–7. From figure 5(*a*), one can readily appreciate how strongly the boundary-layer thickness grows when approaching the pole. We also observe that the quantity $-\partial v_\mu^{(s)}/\partial y$ at $y = 0$ is positive in the beginning, which corresponds to a growing j_{mom},

https://doi.org/10.1017/S0022112003007122 Published online by Cambridge University Press

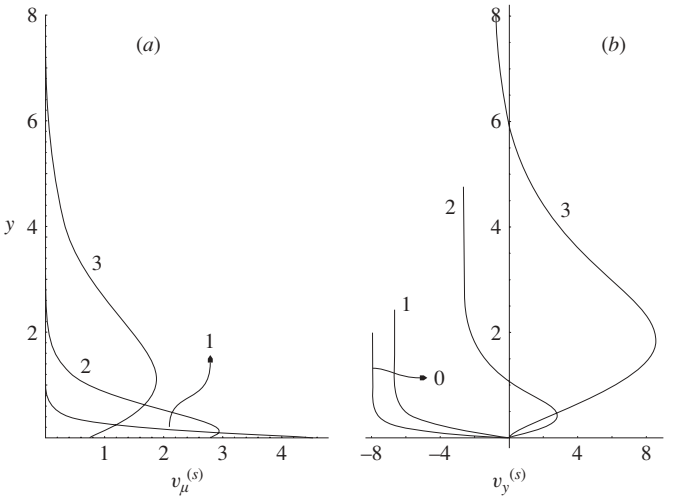


FIGURE 5. Boundary-layer profiles of (*a*) the tangential velocity and (*b*) the normal velocity vs the normal coordinate. The results shown are for the spheroid with aspect ratio $b/a = 1/2$. The numbering of the curves corresponds to the following locations along the surface: '0' for $\mu = 0$ ($s = 0$, the equator), '1' for $\mu = 0.2$ ($s = 0.0848$), '2' for $\mu = 0.6$ ($s = 0.310$), and '3' for $\mu = 0.9$ ($s = 0.637$).

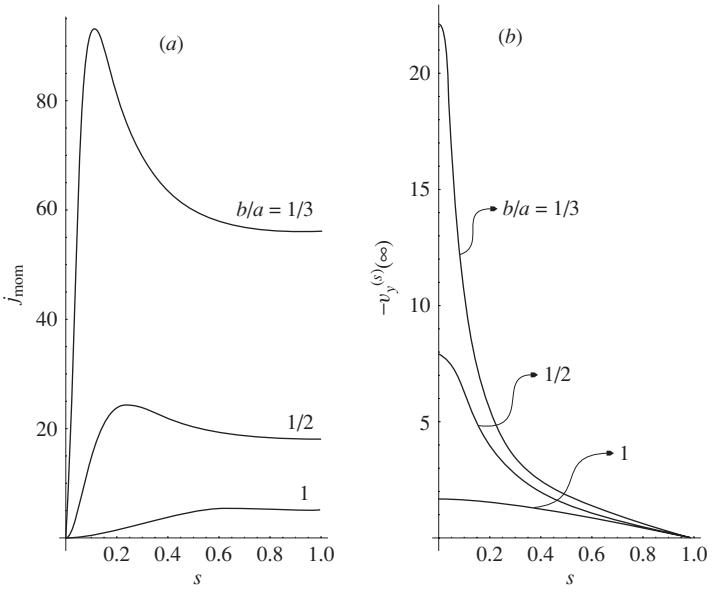


FIGURE 6. Distributions of (*a*) the momentum flux, equation (79), and (*b*) the entrainment velocity along the boundary layer for various aspect ratios.

figure 6(*a*). Then it changes sign, so that the tangential surface stress now formally decelerates the flow, and the momentum flux decreases. The effect of deceleration takes place because the effective slip velocity, which is actually the driving factor behind the streaming flow, starts to decrease past a certain position along the boundary layer and cannot keep pace with the flow accelerated earlier. The smaller the aspect ratio, the more drastic the effect, namely, the greater becomes the difference, in both

https://doi.org/10.1017/S0022112003007122 Published online by Cambridge University Press

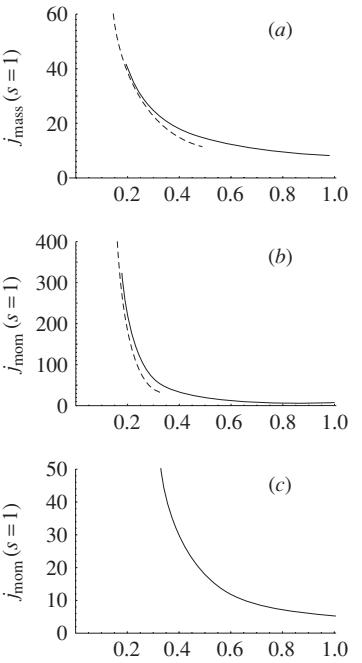


FIGURE 7. (*a*) The mass and (*b*) momentum fluxes at the exit from the boundary layer, equations (78) and (79) taken at $\mu = 1$, as a function of the aspect ratio. Shown in (*c*) is an enlarged view of (*b*) for relatively low values of $j_{\mathrm{mom}}(1)$. The dashed curves correspond to the asymptotic consideration in the disk limit, equation (114) with (7), (8) and (30).

absolute and relative terms, between the maximal value of j_{mom} and its value at the pole, $\mu = s = 1$. At the same time, the location of the maximum shifts closer to the beginning (i.e. to the equator, $\mu = s = 0$). Overall, the tendency is that all the intensities grow with decreasing aspect ratio, while the meaningful initial length scale shrinks. It was found to be so in the Stokes layer (§4), and nothing in the outer boundary-layer dynamics alters the tendency.

Unlike the momentum flux, the mass flux monotonically increases downstream, as the entrainment velocity, shown in figure 6(*b*), is always positive (i.e. it is really an entrainment). And it could not be otherwise, for the behaviour of the solution as $y \to \infty$ is

$$v_{\mu}^{(s)} \propto \exp\left[v_{y}^{(s)}(\mu, \infty)\, y\right]$$

as follows from equation (74), and so $v_{y}^{(s)}(\mu, \infty) < 0$ to ensure an exponential decay as $y \to \infty$. Besides, from here we see that the fact observable in figure 6(*b*) that $v_{y}^{(s)}(s, \infty) = O(1 - s) = O(\delta)$ as $s \to 1$ ($\delta \to 0$) is consistent with the earlier mentioned scaling $y = O(\delta^{-1})$ for the thickness of the boundary layer. As illustrated by figure 5(*b*), the normal velocity is initially negative throughout the whole cross-section of the boundary layer. However, further downstream, a zone of positive normal velocity emerges and grows, and so does the velocity magnitude. Its positivity and growing magnitude, consistent with the scaling mentioned earlier, $v_{y}^{(s)} = O(\delta^{-2})$ as $\delta \to 0$, are precursors for the eventual jet eruption in an asymptotically close vicinity of the pole, where the boundary layer approximation ceases to be valid. However, it follows from the asymptotic development by Amin & Riley (1990) that this leading-order part of

https://doi.org/10.1017/S0022112003007122 Published online by Cambridge University Press

$v_y^{(s)}$ tends to zero as $y \to \infty$. The behaviour at $y \to \infty$ is determined by asymptotically smaller terms, which render $v_y^{(s)}(s, \infty)$ negative, in accordance with figure 6(*b*).

Now we turn to the flow outside the boundary layer, and first discuss the jets. The discussion follows Amin & Riley (1990). The asymptotic scaling for the jet is closely related to that for the singularity in the boundary-layer solution when approaching the poles. The boundary layer can be considered to detach into the jet when the tangential and normal velocities become of the same order of magnitude. In (73)–(76), the velocity components are scaled differently, so that both $v_\mu^{(s)} = O(1)$ and $v_y^{(s)} = O(1)$. However, if they had the same scaling then when the former is $O(1)$, the latter would be $O(R_s^{-1/2})$, which is to be multiplied by $O(\delta^{-2})$ for the vicinity of the pole. Consequently, the jet forms when $R_s^{-1/2}\delta^{-2} = O(1)$, or $\delta = O(R_s^{-1/4})$, which determines the radius of the jet. The velocity component along the jet is $O(1)$, but its radius is much greater than $O(R_s^{-1/2})$ which represents the classical boundary-layer thickness. Therefore, the jet is effectively inviscid over $O(1)$ distances along itself, i.e. on the length scale of the body. It is only at much greater distances, $O(R_s^{1/2})$, that the viscous effects become apparent. From continuity considerations, this yields $O(R_s^{-3/4})$ for the scale of the normal velocity in the jet, which is much smaller than the corresponding scale in the boundary layer, $O(R_s^{-1/2})$. Flow in the main bulk of the fluid, outside the surface boundary layer and the jet, is irrotational. It is caused by the entrainment into the boundary layer and into the jet. But the established scalings clearly show that the former is asymptotically stronger than the latter. Consequently, to leading order, the entrainment into the jet can be neglected here. Having numerically computed $v_y^{(s)}(\mu, \infty)$, we are ready to determine the flow in the main bulk. As a side remark, note that the situation is completely different for the streaming flow in the main bulk of the fluid around a cylinder (calculated by Riley 1975), where all the scalings for the (planar) jet are exactly the same as for the surface boundary layer, and the entrainment into the jet cannot be disregarded.

Thus, turning to the irrotational flow in the main bulk of the fluid, we rescale

$$\psi^{(s)} = R_s^{-1/2}\,\psi_1^{(s)} \tag{80}$$

so that $\psi_1^{(s)} = O(1)$, and the problem for $\psi_1^{(s)}$ is

$$\mathrm{E}^2\psi_1^{(s)} = 0, \tag{81}$$

$$\lambda \to \infty\colon \quad \psi_1^{(s)}/\lambda^2 \to 0, \tag{82}$$

$$\lambda = \lambda_0\colon \quad \psi_1^{(s)} = j_{\mathrm{mass}}(\mu)/(2\pi), \tag{83}$$

$$\mu = \pm 1\colon \quad \partial\psi_1^{(s)}/\partial\lambda = 0, \tag{84}$$

with j_{mass} defined in (78). Boundary condition (83) accounts for the entrainment into the surface boundary layer, while (84) states that there is no entrainment into the jet. In view of (83), condition (84) can be rewritten as $\psi_1^{(s)} = j_{\mathrm{mass}}(\pm 1)/(2\pi)$ at $\mu = \pm 1$, respectively.

Using developments from § 6 and Appendix B, the solution of (81)–(84) can be written as

$$\psi_1^{(s)} = c_1\,\mu + \sum_{n=3}^{\infty}{}' c_n\,\tilde{H}_n(\lambda)\,G_n(\mu) \tag{85}$$

where, in view of the symmetry, only the odd-numbered modes are present, and the prime at the summation symbol indicates that the summation step is equal to 2. The

https://doi.org/10.1017/S0022112003007122 Published online by Cambridge University Press

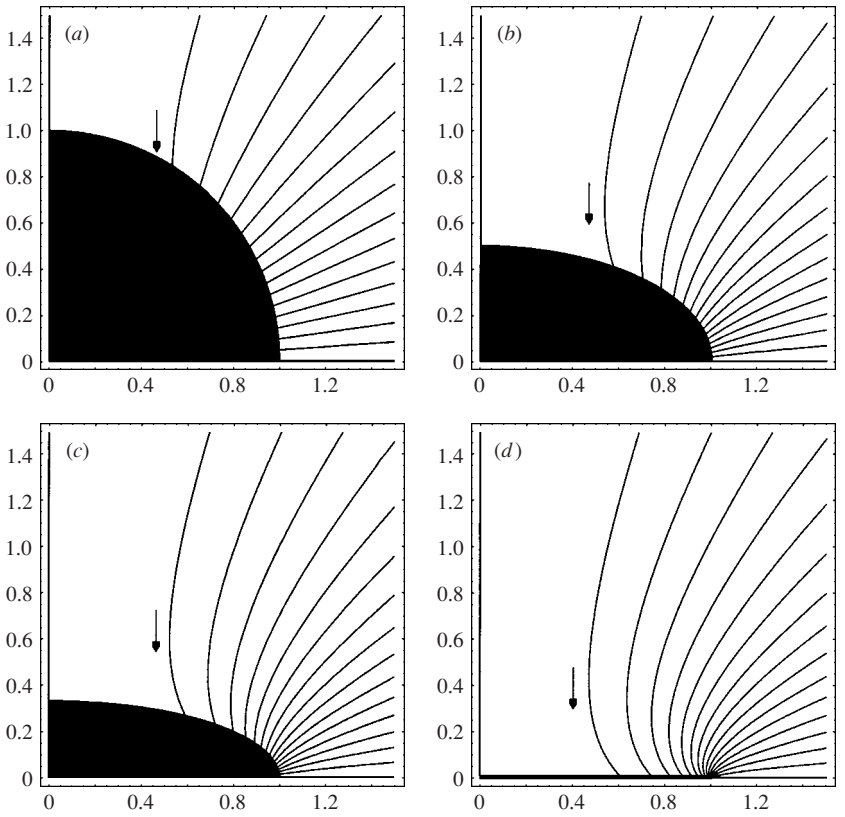


FIGURE 8. The streaming flow in the main bulk of the fluid at large Reynolds number, determined by the entrainment into the surface boundary layer, for various aspect ratios: (*a*) $b/a = 1$, (*b*) $b/a = 1/2$, (*c*) $b/a = 1/3$, and (*d*) $b/a = 0$ (results of the disk asymptotics). The arrows indicate direction of the flow. The streamlines are drawn at the intervals $0.0785R_s^{-1/2}$, $0.145R_s^{-1/2}$, $0.225R_s^{-1/2}$ and $0.0457A\lambda_0^{-3}\bar{R}_s^{-1/2}$ for the above four cases, respectively. See equations (80), (85)–(87) for (*a–c*) and (115)–(118) for (*d*) with (7), (8), (30), (48) and (104).

coefficients are

$$c_1 = \frac{j_{\mathrm{mass}}(1)}{2\pi}, \tag{86}$$

$$c_n = \frac{n(n-1)(2n-1)}{2\pi\,\tilde{H}_n(\lambda_0)} \int_0^1 \frac{j_{\mathrm{mass}}(\mu) - \mu\, j_{\mathrm{mass}}(1)}{1-\mu^2}\, G_n(\mu)\,\mathrm{d}\mu \qquad (n = 3, 5, \ldots). \tag{87}$$

When deriving (87), formula (C 1) from Appendix C has been used.

Thus, the potential steady streaming flow outside the surface boundary layer and the jet is given by (80), (85)–(87). The streamlines are shown in figure 8(*a–c*) for various aspect ratios of the oblate spheroid. Figure 8(*d*) corresponds to the disk limit to be considered in the next section.

8. The disk limit

Here we are concerned with the asymptotic limit of a disk, $\lambda_0 \to 0$, within the boundary-layer consideration of the previous section. An important starting point is the behaviour as $\lambda_0 \to 0$ of the effective slip velocity, equation (34), which is the

https://doi.org/10.1017/S0022112003007122 Published online by Cambridge University Press

only driving factor in the problem (73)–(76). As has been already been pointed out in equation (37), its peak distribution, of magnitude $O(\lambda_0^{-4})$, belongs to an asymptotically small region near the sharp-edged equator, where $\mu = O(\lambda_0)$, or $x = O(\lambda_0^2)$ in terms of (36). In this region, we have $v_\mu^{(s)} = O(\lambda_0^{-4})$. Also, from (73)–(76), it can be established that $v_y^{(s)} = O(\lambda_0^{-3})$ and $y = O(\lambda_0^3)$. The appropriate streaming Reynolds number for this localized flow has been defined in (50). The boundary-layer consideration is valid for $\tilde{R}_s \gg 1$, which in view of $\lambda_0 \ll 1$ does not necessarily require R_s to be large.

Downstream of that tiny initial region lies the main part of the boundary layer, where the slip velocity decays quite fast. No longer receiving a sufficient push from the boundary, the flow intensity also decays, but not as fast as the slip velocity, as we will see later. In the present asymptotic approach, we separate the boundary layer into two zones. The first (initial) zone is located at $0 < \mu < O(\lambda_0)$, or $0 < x < O(\lambda_0^2)$, while the second (main) zone corresponds to $O(\lambda_0) \ll \mu < 1$, or $O(\lambda_0^2) \ll x < x(1)$ (notice that $x(1) = 1$ in the limit $\lambda_0 \to 0$). After solving for the first zone, initial conditions for the second one are inferred from the region of their overlap, which corresponds to an intermediate asymptotics between the zones.

In the first zone, using the scaling established earlier, we rescale the variables so that the new quantities, marked with a tilde, are all $O(1)$:

$$\mu = \lambda_0 \tilde{\mu}, \quad x = \lambda_0^2 \tilde{x}, \quad v_\mu^{(s)} = A^2 \lambda_0^{-4} \tilde{v}_\mu^{(s)}, \quad y = A^{-1} \lambda_0^3 \tilde{y}, \quad v_y^{(s)} = A \lambda_0^{-3} \tilde{v}_y^{(s)}. \tag{88}$$

Then, to leading order, the problem (73)–(76) becomes

$$\frac{1}{(1+\tilde{\mu}^2)^{1/2}} \frac{\partial \tilde{v}_\mu^{(s)}}{\partial \tilde{\mu}} + \frac{\partial \tilde{v}_y^{(s)}}{\partial \tilde{y}} = 0, \tag{89}$$

$$\frac{1}{(1+\tilde{\mu}^2)^{1/2}} \tilde{v}_\mu^{(s)} \frac{\partial \tilde{v}_\mu^{(s)}}{\partial \tilde{\mu}} + \tilde{v}_y^{(s)} \frac{\partial \tilde{v}_\mu^{(s)}}{\partial \tilde{y}} = \frac{\partial^2 \tilde{v}_\mu^{(s)}}{\partial \tilde{y}^2}, \tag{90}$$

$$\tilde{y} \to \infty: \quad \tilde{v}_\mu^{(s)} \to 0, \tag{91}$$

$$\tilde{y} = 0: \quad \tilde{v}_\mu^{(s)} = \frac{3}{4} \frac{\tilde{\mu}}{(1+\tilde{\mu}^2)^{5/2}}, \quad \tilde{v}_y^{(s)} = 0. \tag{92}$$

As the size of the zone is much smaller than the distance to the symmetry axis, the problem (89)–(92) is effectively planar. Equations (89) and (90) would be more compact in terms of the variable

$$\tilde{x} = \tfrac{1}{2} \operatorname{arcsinh} \tilde{\mu} + \tfrac{1}{2} \tilde{\mu} (1+\tilde{\mu}^2)^{1/2}$$

and we would have

$$\frac{1}{(1+\tilde{\mu}^2)^{1/2}} \frac{\partial}{\partial \tilde{\mu}} = \frac{\partial}{\partial \tilde{x}}, \qquad \tilde{v}_\mu^{(s)} \equiv \tilde{v}_x^{(s)}, \tag{93}$$

where the latter redefinition of the tangential velocity would be appropriate for consistency of notation. However, as (92) is given in terms of $\tilde{\mu}$, we have kept equations (89) and (90).

Notice that the coefficient A, given by equation (30), has been incorporated into the rescaling (88), and is not present explicitly in (89)–(92). Within the leading-order approach, we could have set $A = 2/\pi$ which results from (30) at $\lambda_0 = 0$. However, there is a reason why we prefer to retain the general form of A: the principal correction, of relative order $O(\lambda_0)$, to the leading-order consideration comes virtually only from A, as all other possible sources of corrections yield them of higher asymptotic order than $O(\lambda_0)$. Thus, keeping A permits us to automatically account for the principal correction. In fact, it is so only provided that $R_s \gg 1$; for if $R_s = O(1)$ then as

https://doi.org/10.1017/S0022112003007122 Published online by Cambridge University Press

seen from (50) the correction due to the boundary-layer approximation itself would be $O(\tilde{R}_s^{-1/2}) = O(\lambda_0)$, i.e. of the same order of magnitude as from A. In any case, retaining A does not cause problems, as with (88) it is successfully scaled out of the formulation, which becomes free of any parameters.

The problem (89)–(92) is integrated numerically using a stepwise procedure similar to that in the previous section. The integration starts at $\tilde{\mu} = 0$, where the initial condition $\tilde{v}_\mu^{(s)} = 0$ is imposed, and may go up to any value of $\tilde{\mu}$. In order to proceed further with the second (main) zone of the boundary layer, we need to know the asymptotic behaviour of the solution at large values of $\tilde{\mu}$.

For the purpose of determining this asymptotic behaviour, it is more convenient to work in terms of $\tilde{x}$, and below it is implicit that equations (89) and (90) are rewritten with the help of (93). Also, we note that $\tilde{x} = \tilde{\mu}^2/2 + O(\ln\tilde{\mu})$ at $\tilde{\mu} \gg 1$. We expect that at $\tilde{x} \gg 1$ the solution attains a self-similar form. We write

$$\eta = \frac{\tilde{y}}{\tilde{x}^{(1-\alpha)/2}}, \quad \tilde{v}_x^{(s)} = \tilde{x}^\alpha f(\eta), \quad \tilde{v}_y^{(s)} = \tilde{x}^{(\alpha-1)/2} g(\eta) \tag{94}$$

where α is to be established. The continuity equation (89) is identically satisfied with

$$f(\eta) = \frac{\partial G}{\partial \eta}, \quad g(\eta) = -\tfrac{1}{2}(\alpha+1)\, G + \tfrac{1}{2}(1-\alpha)\eta \frac{\partial G}{\partial \eta} \tag{95}$$

where $G = G(\eta)$. Notice that

$$\tilde{x}^{(\alpha+1)/2} G(\eta)$$

plays the role of the stream function for the planar flow governed by (89) and (90).

On using (93)–(95) in (90)–(92), the following problem for $G(\eta)$ results:

$$\alpha \left(\frac{\partial G}{\partial \eta}\right)^2 - \tfrac{1}{2}(\alpha+1) G \frac{\partial^2 G}{\partial \eta^2} = \frac{\partial^3 G}{\partial \eta^3}, \tag{96}$$

$$\eta \to \infty: \quad \frac{\partial G}{\partial \eta} \to 0, \tag{97}$$

$$\eta = 0: \quad G = 0, \tag{98}$$

but it remains to be seen how the first condition (92) is to be incorporated. With the self-similar behaviour postulated, one possibility is to set $\alpha = -2$ with the condition becoming

$$\eta = 0: \quad \frac{\partial G}{\partial \eta} = \frac{3}{16}. \tag{99}$$

However, in accordance with Banks (1983), the solution of the boundary-value problem (96)–(99) does not exist for $\alpha = -2$ and at the same time a positive value of the right-hand side of (99).

Another possibility is to consider (96)–(98) with the trivial boundary condition

$$\eta = 0: \quad \frac{\partial G}{\partial \eta} = 0, \tag{100}$$

where $\alpha > -2$ for consistency in neglecting the effective slip velocity within the $\tilde{x} \gg 1$ ($\tilde{\mu} \gg 1$) asymptotics. As the problem (96)–(98) and (100) always allows the trivial solution, α is an eigenvalue and should be such that a non-trivial solution exists. Besides, we note that we are only interested in solutions with an exponential decay of $\partial G/\partial \eta$ as $\eta \to \infty$. The appropriate value of α is

$$\alpha = -\tfrac{1}{2} \tag{101}$$

https://doi.org/10.1017/S0022112003007122 Published online by Cambridge University Press

and the corresponding self-similar boundary-layer solution is known as the planar wall jet (Akatnov 1953; Glauert 1956). With (101), there exists a one-parameter family of solutions: let $G_0(\eta)$ be the solution of the problem

$$-\frac{1}{2}\left(\frac{\partial G_0}{\partial \eta}\right)^2 - \frac{1}{4}G_0\frac{\partial^2 G_0}{\partial \eta^2} = \frac{\partial^3 G_0}{\partial \eta^3},$$

$$\eta \to \infty: \quad \frac{\partial G_0}{\partial \eta} \to 0,$$

$$\eta = 0: \qquad G_0 = 0, \quad \frac{\partial G_0}{\partial \eta} = 0, \quad \frac{\partial^2 G_0}{\partial \eta^2} \equiv 1,$$

where the last condition is formally added to single out a particular solution (a kind of normalization). Then, any solution of (96)–(98) and (100) with (101) is given by

$$G(\eta) = \tau^{1/3} G_0\left(\tau^{1/3}\eta\right) \tag{102}$$

with $\tau > 0$ being the parameter of the family, which characterizes the intensity of the wall jet. We see that $\tau = \partial^2 G/\partial \eta^2$ at $\eta = 0$.

Thus, we expect that the boundary-layer flow asymptotically approaches the wall jet far downstream of the initial zone, which is represented by (94), (95), (101) and (102). A direct numerical computation of the problem (89)–(92) confirms this, and also yields the value

$$\tau = 0.0124. \tag{103}$$

The wall-jet asymptotics is made possible by a fast downstream decay of the effective slip velocity at the surface – fast compared to the decay for the wall jet itself.

In the planar counterpart of the oblate spheroidal problem, the wall-jet form of the flow would have lasted up to the collision point at the symmetry line (the analogue of the symmetry axis here). This is not so in the axisymmetric formulation, where the planar wall jet is only an intermediate asymptotics between the zones with $x = O(\lambda_0^2)$ and $x = O(1)$ (respectively $\mu = O(\lambda_0)$ and $\mu = O(1)$ in terms of μ). It undergoes an appreciable geometric distortion in the main zone to finally result in the singularity at the symmetry axis in the same way as described in § 7.

Below we consider the flow in the main zone of the boundary layer, $O(\lambda_0^2) \ll x < 1$ ($O(\lambda_0) \ll \mu < 1$). We work in terms of the coordinate x, which is $x = [1-(1-\mu^2)^{1/2}]$ in the limit $\lambda_0 \to 0$. Also, for consistency, we rename the tangential velocity component: $v_\mu^{(s)} \equiv v_x^{(s)}$.

The scaling with λ_0 for the boundary-layer flow in the main zone is fully determined by the necessity of matching with the wall-jet asymptotics as $x \to 0$. With (88), (94) and (101), we deduce the following boundary-layer scalings: $v_x^{(s)} = O(\lambda_0^{-3})$, $y = O(\lambda_0^{3/2})$ and $v_y = O(\lambda_0^{-3/2})$. Naturally, the value of the velocity is much smaller than that for the initial zone, but it is however much greater than the effective slip velocity, which is $O(1)$ in the main zone. Just as in (50), we can introduce a quantity to serve as the streaming Reynolds number for the main zone: R_s multiplied by the scale $v_x^{(s)}x = O(\lambda_0^{-3})$, i.e.

$$\bar{R}_s = \frac{R_s}{\lambda_0^3}. \tag{104}$$

Despite a smaller velocity scale in the main zone, the magnitude of (104) is much greater than its counterpart (50) in the initial zone. This is due to the relative size of the zones. For the present boundary-layer consideration to be valid, it is sufficient to demand $\tilde{R}_s \gg 1$. Then $\bar{R}_s \gg 1$ follows automatically.

https://doi.org/10.1017/S0022112003007122 Published online by Cambridge University Press

With the scalings established, the appropriate counterpart of (88) is

$$v_x^{(s)} = A^2\lambda_0^{-3}\,\bar{v}_x^{(s)}, \quad y = A^{-1}\lambda_0^{3/2}\,\bar{y}, \quad v_y^{(s)} = A\lambda_0^{-3/2}\,\bar{v}_y^{(s)}, \tag{105}$$

where the new quantities, marked with a bar, are $O(1)$ in the main zone. No rescaling is needed for x which is already an $O(1)$ quantity. The coefficient A is carried through in the same way as it was for the initial zone. Then, in the limit $\lambda_0 \to 0$, the problem (73)–(76) reduces to

$$\frac{1}{1-x}\frac{\partial}{\partial x}\left[(1-x)\bar{v}_x^{(s)}\right] + \frac{\partial \bar{v}_y^{(s)}}{\partial \bar{y}} = 0, \tag{106}$$

$$\bar{v}_x^{(s)}\frac{\partial \bar{v}_x^{(s)}}{\partial x} + \bar{v}_y^{(s)}\frac{\partial \bar{v}_x^{(s)}}{\partial \bar{y}} = \frac{\partial^2 \bar{v}_x^{(s)}}{\partial \bar{y}^2}, \tag{107}$$

$$\bar{y} \to \infty: \quad \bar{v}_x^{(s)} \to 0, \tag{108}$$

$$\bar{y} = 0: \quad \bar{v}_x^{(s)} = \bar{v}_y^{(s)} = 0. \tag{109}$$

The initial condition for the main zone is given by the wall jet that develops at the exit from the initial zone. It can be written as

$$x \to 0: \quad \bar{v}_x^{(s)} \to \frac{1}{x^{1/2}}\,f\left(\frac{\bar{y}}{x^{3/4}}\right), \tag{110}$$

where the function f is defined by (95) and (101)–(103).

As the initial condition is given in the asymptotic form, with the velocity diverging but the boundary-layer thickness shrinking to zero as $x \to 0$, it is convenient to recast (106)–(110) in terms of the variables $\bar{y}/x^{3/4}$, $x^{1/2}\bar{v}_x^{(s)}$ and $x^{3/4}\bar{v}_y^{(s)}$ instead of $\bar{y}$, $\bar{v}_x^{(s)}$ and $\bar{v}_y^{(s)}$. A stepwise numerical integration, similar to § 7, is then carried out by proceeding from $x = 0$ towards $x = 1$ and stopping slightly short of approaching the symmetry axis, $x = 1$, where the singularity occurs.

The form of equations (106) and (107) reveals that they belong to the disk limit. This can be made more apparent if we note that, to the same approximation that (106) and (107) result from (73) and (74), we have $(1-x) = \varrho$ and $\bar{v}_x^{(s)} = -\bar{v}_\varrho^{(s)}$, where $\bar{v}_\varrho^{(s)}$ is the (rescaled) radial velocity component in the cylindrical coordinates. With the above replacements, (106)–(109) clearly becomes an axisymmetric boundary-layer problem in the cylindrical coordinates over a flat disk surface. The flow is excited by the wall jet that is initiated at the edge of the disk and blows inside. As will be discussed later, it is only the intensity of the wall jet that bears any resemblance to the particulars of the body shape (i.e. the oblate spheroid in our case).

The mass and momentum fluxes (78) and (79) are rescaled following (105):

$$j_{\mathrm{mass}} = \frac{A}{\lambda_0^{3/2}}\,\bar{j}_{\mathrm{mass}}, \quad j_{\mathrm{mom}} = \frac{A^3}{\lambda_0^{9/2}}\,\bar{j}_{\mathrm{mom}}, \tag{111}$$

where

$$\bar{j}_{\mathrm{mass}}(x) = 2\pi(1-x)\int_0^\infty \bar{v}_x^{(s)}\,\mathrm{d}\bar{y} = -2\pi\int_0^x (1-x')\bar{v}_y^{(s)}(x',\infty)\,\mathrm{d}x', \tag{112}$$

$$\bar{j}_{\mathrm{mom}}(x) = 2\pi(1-x)\int_0^\infty \left(\bar{v}_x^{(s)}\right)^2\mathrm{d}\bar{y}. \tag{113}$$

In view of (110), the momentum flux can be seen to diverge as $\bar{j}_{\mathrm{mom}} = O(x^{-1/4})$ as $x \to 0$. This simply reflects the fact that asymptotically higher values of j_{mom} are attained in the initial zone of the boundary layer, where the streaming flow is

https://doi.org/10.1017/S0022112003007122 Published online by Cambridge University Press

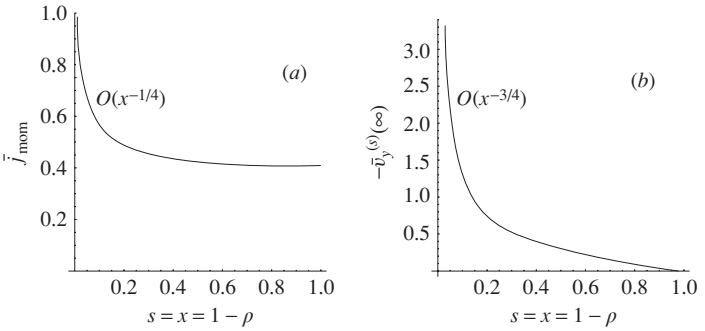


FIGURE 9. Distributions of the rescaled (*a*) momentum flux and (*b*) entrainment velocity along the boundary layer in the disk limit. See equations (105) and (111) with (30).

generated. Then, due to the friction from the boundary, $j_{\rm mom}$ falls to an asymptotically lower value. Due to this divergence, the second expression (79) cannot be substituted in (113). But, of course, a similar relation can be written between any two stations with $x > 0$, i.e.

$$\bar{j}_{\rm mom}(x_2) - \bar{j}_{\rm mom}(x_1) = -2\pi \int_{x_1}^{x_2} (1 - x') \frac{\partial \bar{v}_x^{(s)}}{\partial \bar{y}}(x', 0)\, {\rm d}x'$$

where $0 < x_1 < 1$ and $0 < x_2 < 1$.

The situation is different for the mass flux. The divergence of the entrainment velocity like $O(x^{-3/4})$ as $x \to 0$ is integrable and yields $\bar{j}_{\rm mass} = O(x^{1/4})$ as $x \to 0$. This shows that the contribution to the mass flux in the initial zone is small, and almost all the entrainment into the boundary layer occurs in the main zone.

Some numerical results for the main zone are represented in figure 9(*a*, *b*), where the (rescaled) momentum flux and the entrainment velocity are shown. The mass flux can be obtained from the latter by means of (112). Note also that the computation yields the values $\bar{j}_{\rm mass}(1) = 4.60$ and $\bar{j}_{\rm mom}(1) = 0.408$. In view of (111), this leads to

$$j_{\rm mass}(1) = 4.60\, \frac{A}{\lambda_0^{3/2}}, \qquad j_{\rm mom}(1) = 0.408\, \frac{A^3}{\lambda_0^{9/2}}, \tag{114}$$

where A is as in (30). Equations (114) represent the $\lambda_0 \ll 1$ asymptotics for the mass and momentum fluxes at the exit from the boundary layer, namely at the pole, where the boundary-layer flow self-collides to form a circular jet emanating from the body along the symmetry axis. The results (114), taking (7), (8) and (30) into account, are shown in figure 7 by dashed lines, and are in a reasonably good agreement with the results of § 7 (solid lines) at relatively low aspect ratios of the oblate spheroid.

Regarding the singularity at the poles and the resulting circular jet, we only need to mention that the geometric scaling estimations pointed out in § 7 in terms of R_s are *verbatim* valid here in terms of $\bar{R}_s$, defined in (104). In particular, the radius of the jet scales as $O(\bar{R}_s^{-1/4})$, while the distance along the jet over which the viscous effects are important is $O(\bar{R}_s^{1/2})$ (recall the distance is that in the units of the disk radius, the large semi-axis of the oblate spheroid). The entrainment into the jet remains negligible compared to that into the boundary layer.

The irrotational flow in the main body of the fluid, outside the boundary layer and the jet, is determined by the entrainment into the boundary layer, and more precisely into its main zone as far as the disk limit is concerned. This flow can be found in the

https://doi.org/10.1017/S0022112003007122 Published online by Cambridge University Press

same way as in § 7, with expressions (80) and (85)–(87) becoming

$$\psi^{(s)} = A\,\lambda_0^{-3}\,\bar{R}_s^{-1/2}\,\bar{\psi}_1^{(s)}, \tag{115}$$

$$\bar{\psi}_1^{(s)} = \bar{c}_1\,\mu + {\sum_{n=3}^{\infty}}'\bar{c}_n\,\tilde{H}_n(\lambda)\,G_n(\mu), \tag{116}$$

$$\bar{c}_1 = \frac{\bar{j}_{\mathrm{mass}}(1)}{2\pi}, \tag{117}$$

$$\bar{c}_n = \frac{n(n-1)(2n-1)}{2\pi\,\tilde{H}_n(\lambda_0)}\int_0^1 \frac{\bar{j}_{\mathrm{mass}}(\mu)-\mu\,\bar{j}_{\mathrm{mass}}(1)}{1-\mu^2}\,G_n(\mu)\,\mathrm{d}\mu \qquad (n=3,5,\ldots), \tag{118}$$

where $\bar{j}_{\mathrm{mass}}(x)$ is known from the numerical computation in the boundary layer. To rewrite it in terms of μ, we note that $x = [1-(1-\mu^2)^{1/2}]$ in the limit $\lambda_0 \to 0$. The flow (115)–(118) is shown in figure 8(*d*). When making this plot, we disregard a possible relative $O(\lambda_0)$ correction, which now does not enter solely through A, and therefore set $\lambda_0 = 0$ in (118).

Thus far, it has been implied that the disk limit is approached while remaining within the family of oblate spheroids. In fact, from the standpoint of steady streaming, the disk limit does not exist unless a particular one-parametric family of body shapes is specified such that the body becomes a disk as the parameter goes to zero (the parameter can always be conveniently chosen in this way if the disk shape is attainable within the family). In other words, the disk limit is not absolute, but shape-dependent. Now, still remaining within the disk approximation, we shall consider implications of the results of the present section for families other than the oblate spheroids. We restrict our consideration to the class of smooth-edged disk-like bodies (see the end of § 4). First, the qualitative features established here for the oblate spheroid are expected to hold. In particular, this concerns separation into the initial and main zones of the boundary layer and scaling of all the quantities with λ_0, where λ_0 should now be understood as $\lambda_0 \propto \mathscr{R}_c^{1/2} \ll 1$ according to (38). As a more quantitative observation, we note that the form of the main-zone formulation (105)–(110) is not to change. It has already been pointed out that (106)–(110) has lost any resemblance to the shape specifics and has the appearance of a boundary-layer problem over a flat disk surface. Regarding (105), we just note that, beyond the oblate spheroidal case, it would not make sense to keep A as a function of λ_0, which was done with the aim of accounting for the leading correction, of the relative order $O(\lambda_0)$. Instead, we set $A = 2/\pi$ as follows from (30) at $\lambda_0 = 0$ (perhaps it would be more natural to set $A = 1$, but we choose $A = 2/\pi$ to be consistent with the notation). All that will change in (105)–(110) is the intensity of the wall jet in (110), where recall that f is given by (95), (101) and (102). Thus, all the specifics of a particular shape are accounted for in a single parameter τ. It is given by (103) for oblate spheroids, and is generally different for other shapes. The wall-jet intensity is determined by the boundary-layer flow development in the initial zone, where a particular distribution of the effective slip velocity depends on details of the body shape. If a disk-like body is not symmetric with respect to the equatorial plane, the values of τ will naturally be different on different sides of the disk. It is worthwhile to mention that, to leading order, the body shape matters only in a close vicinity of the edge, over $O(\mathscr{R}_c)$ distances. For example, if a disk-like body has a paraboloidal edge then, irrespective of its shape in the middle, the steady streaming is, to leading order, the same as for an oblate spheroid with the same edge parabola.

https://doi.org/10.1017/S0022112003007122 Published online by Cambridge University Press

9. Summary and concluding remarks

We have studied the steady streaming appearing when an oblate spheroid performs small-amplitude high-frequency (see (3) and (4)) translational oscillations parallel to its symmetry axis and relative to an incompressible host fluid. The main definitions and notation are given in (3)–(9), (14), (17), (30) and (36). The flow field is represented as a superposition of unsteady and steady parts, as in (21), separately in the (asymptotically thin) Stokes layer at the body surface and the main bulk of the fluid outside the Stokes layer. Solutions in the two regions are connected by the matching requirement. Our analysis has focused on obtaining a leading-order result for the steady part (steady streaming). In view of the symmetry of the problem, all steady distributions and fields, apart from being axisymmetric, are symmetric with respect to the equatorial plane of the spheroid.

The inner streaming (in the Stokes layer) is given by (33) and illustrated in figure 3. The flow does not fade away at the outer edge of the Stokes layer and results in, on the scale of the main bulk of the fluid, the effective slip velocity at the body surface, given by (34) and illustrated in figure 2. The slip velocity is always directed from the equator of the oblate spheroid towards its poles.

The outer streaming (in the main bulk of the fluid) is governed by the steady Navier–Stokes equation (47), with the streaming Reynolds number defined in (48), and boundary conditions (35) and (49), where the effective slip velocity in (35) is the only driving factor. That it is the ordinary (without additional terms) steady Navier–Stokes equation, as well as that the Eulerian mean flow is not different from the Lagrangian one and does not depend on whether the particle or the fluid medium is at rest in the laboratory frame of reference, are consequences of the leading-order oscillatory flow having a single phase in the outer region.

In the limit of a small streaming Reynolds number, the Stokes (creeping flow) solution for the outer streaming is given by (70) with (66), (69) and (71), and the flow patterns are shown in figure 4. Another point of interest here is equation (63), which is the most general form of the Stokes solution not implying velocity singularities at the symmetry axis. It may be useful for other problems in the oblate spheroidal geometry. We have pointed out an asymmetry in (63) with respect to the exterior and interior problems.

At a large streaming Reynolds number, the outer streaming has a boundary-layer structure over the body surface, the boundary layer being always much thicker than the Stokes layer. The solution has been obtained numerically. Some results are shown in figures 5–7, while the relevant definitions are in (72), (78) and (79). The boundary-layer flow has been found to proceed smoothly, for all aspect ratios of the oblate spheroid, from the equator to the poles, where it meets a geometric singularity. Upon its self-collision at the poles, the flow is expected to turn around to form circular jets emanating from the body along the symmetry axis. Outside the boundary layer and the jets, the steady flow is potential and of asymptotically lower intensity. It is fully determined by the entrainment into the boundary layer as that into the jets is negligibly small. The result is given by (80) and (85)–(87) and illustrated in figure 8.

Topologically, the steady streaming around an oblate spheroid always looks similar to that for a sphere. However, two tendencies become apparent as the aspect ratio is decreased (while the amplitude of oscillations and the major radius remain constant). First, the streaming intensity grows appreciably. Second, the zone of most intense streaming shrinks and localizes in a smaller and smaller vicinity of the equator.

https://doi.org/10.1017/S0022112003007122 Published online by Cambridge University Press

The above two tendencies are further underscored by our analysis in the limit of a small aspect ratio (the disk limit; however the amplitude of oscillations and the thickness of the Stokes layer are still assumed much smaller than any linear size of the body). They can clearly be observed from the velocity and coordinate scaling, equation (37), in a narrow near-equator zone of the most intense streaming (zone *I*, or the initial zone), where note that the coordinate scaling characterizes both the distance from the equator and the size of the zone. The geometric size of zone *I* proves to be of the order of the radius of curvature at the equator of the oblate spheroid (cf. (37) and (38)). Despite an asymptotically small size of the zone, the velocity is so high that the streaming Reynolds number defined locally for zone *I* (see equation (50)) increases on decreasing the aspect ratio. Further away from the equator and up to the pole, in what we refer to as zone *II* or the main zone, the streaming intensity has an asymptotically lower value. The intensity reduction is much more drastic for the inner streaming (and as a consequence the effective slip velocity) than for the outer streaming. Thus, the outer streaming in zone *II* is determined by its natural decay away from zone *I* and is not affected by the effective slip velocity at the body surface, which is then negligible.

The concept of the two zones proves tractable for the outer streaming within the boundary-layer approach corresponding to a large streaming Reynolds number. In zone *II*, to leading order, the boundary-layer flow is over a circular disk with no slip at the surface and is excited by a wall jet coming from along the disk circumference inwards. The wall jet represents the net action of flow acceleration in zone *I* as seen from the standpoint of zone *II*. Scaling for various variables in zones *I* and *II* can be inferred from (88) and (105) respectively, where quantities with a tilde or a bar and A are of order unity as $\lambda_0 \to 0$ (consult (72) for notation). What we obtain from (88) naturally corresponds to (37) already cited above. The streaming Reynolds number in zone *II* is given by (104). Some results pertinent to zone *II* are shown in figures 7 and 9. The integral fluid entrainment into the boundary layer is asymptotically smaller for zone *I* than for zone *II*. Therefore, the potential steady flow outside the boundary layer is determined by the entrainment into zone *II*. The result is given by (115)–(118) and shown in figure 8(*d*).

From the viewpoint of the steady streaming, the disk limit is not universal but, rather, shape-dependent. We have studied it quantitatively for the family of oblate spheroids. The results would be different for other shapes. However, qualitatively, what we have established is expected to hold for other disk-like axisymmetric bodies with smoothly rounded edges. In particular, this concerns the scalings. As we have pointed out, the small parameter through which the oblate spheroid is in asymptotic correspondence with another disk-like body in the disk limit is not the aspect ratio, but rather the ratio of the radius of curvature in the vicinity of the edge to the major radius, i.e. the dimensionless radius of curvature. With (38), all the scalings referred to above can be recast via the dimensionless radius of curvature and, in this form, applied to a broad class of bodies in the disk limit.

Financial support from NASA is gratefully acknowledged.

Appendix A. Derivation of equation (10)

The stream function ψ is introduced according to

$$\boldsymbol{v} = \nabla\times\left(\frac{\boldsymbol{e}_\phi}{\varrho}\psi\right) = \frac{1}{\varrho}(\nabla\psi)\times\boldsymbol{e}_\phi \tag{A 1}$$

https://doi.org/10.1017/S0022112003007122 Published online by Cambridge University Press

so that equation (1) is identically satisfied. Here $\{z, \varrho, \phi\}$ is the cylindrical coordinate system based upon the symmetry axis, and $\boldsymbol{e}_z$, $\boldsymbol{e}_\varrho$ and $\boldsymbol{e}_\phi$ are the corresponding unit vectors.

Next, the pressure is eliminated by taking the curl of equation (2). Now we need to express $\nabla \times \boldsymbol{v}$ in terms of ψ. As the velocity components are independent of ϕ due to axial symmetry, it is clear that the only component of the vector $\nabla \times \boldsymbol{v}$ is in the ϕ-direction, and the operator E^2 is defined as

$$\nabla \times \boldsymbol{v} = \nabla \times \left[\nabla \times \left(\frac{\boldsymbol{e}_\phi}{\varrho} \psi \right) \right] \equiv -\frac{\boldsymbol{e}_\phi}{\varrho} \mathrm{E}^2 \psi. \tag{A 2}$$

Applying the formulæ (A 1) and (A 2) for the second time, we obtain

$$\nabla \times [\nabla \times [\nabla \times \boldsymbol{v}]] = -\nabla \times \left[\nabla \times \left(\frac{\boldsymbol{e}_\phi}{\varrho} \mathrm{E}^2 \psi \right) \right] = \frac{\boldsymbol{e}_\phi}{\varrho} \mathrm{E}^2 \mathrm{E}^2 \psi.$$

Thus, the curl of equation (2), whose only non-zero projection is in the ϕ-direction, can be written as

$$\frac{\partial \mathrm{E}^2 \psi}{\partial t} - \frac{\varepsilon}{\varrho} (\nabla \psi \times \nabla \mathrm{E}^2 \psi) \cdot \boldsymbol{e}_\phi + \frac{2\varepsilon}{\varrho^2} \mathrm{E}^2 \psi (\nabla \psi \times \nabla \varrho) \cdot \boldsymbol{e}_\phi = \frac{1}{M^2} \mathrm{E}^2 \mathrm{E}^2 \psi. \tag{A 3}$$

Now it is not difficult to express the second relation (A 1) and (A 3) in an orthogonal curvilinear coordinate system of revolution, $\{\mu, \lambda, \phi\}$, using $\nabla = \{h_\mu^{-1} \partial/\partial\mu, h_\lambda^{-1} \partial/\partial\lambda, 0\}$ with $\partial/\partial\phi \equiv 0$ where appropriate in view of axial symmetry.

If $\{\mu, \lambda, \phi\}$ are the (modified) oblate spheroidal coordinates, as described in § 2.2, we have

$$h_\mu = \left[\left(\frac{\partial z}{\partial \mu} \right)^2 + \left(\frac{\partial \varrho}{\partial \mu} \right)^2 \right]^{1/2} = \frac{c\,(\lambda^2 + \mu^2)^{1/2}}{(1 - \mu^2)^{1/2}}, \quad h_\lambda = \frac{c\,(\lambda^2 + \mu^2)^{1/2}}{(1 + \lambda^2)^{1/2}}.$$

In this way we see that (A 3) yields (10), while (A 1) yields (9).

Finally, to express the operator E^2, we note that the ϕ-component (the only one) of the curl (A 2) is

$$\frac{1}{h_\mu h_\lambda} \left[\frac{\partial}{\partial \mu} (v_\lambda h_\lambda) - \frac{\partial}{\partial \lambda} (v_\mu h_\mu) \right].$$

From this, with the expressions for the velocity components in terms of the stream function already known, we obtain

$$\mathrm{E}^2 = \frac{\varrho}{h_\lambda h_\mu} \left[\frac{\partial}{\partial \lambda} \left(\frac{h_\mu}{\varrho h_\lambda} \frac{\partial}{\partial \lambda} \right) + \frac{\partial}{\partial \mu} \left(\frac{h_\lambda}{\varrho h_\mu} \frac{\partial}{\partial \mu} \right) \right]$$

which in the oblate spheroidal coordinates becomes as in § 2.2.

Appendix B. The functions $G_n(\mu)$, $\tilde{G}_n(\lambda)$ and $\tilde{H}_n(\lambda)$

For $n = 0$ and $n = 1$ these functions are already cited in (55) and (57). For $n \geqslant 2$ they are

$$G_n(\mu) = -\frac{1}{(n-1)!} \left(\frac{\mathrm{d}}{\mathrm{d}\mu} \right)^{n-2} \left(\frac{\mu^2 - 1}{2} \right)^{n-1},$$

https://doi.org/10.1017/S0022112003007122 Published online by Cambridge University Press

$$\tilde{G}_n(\lambda) = \frac{1}{(n-1)!}\left(\frac{\mathrm{d}}{\mathrm{d}\lambda}\right)^{n-2}\left(\frac{\lambda^2+1}{2}\right)^{n-1},$$

$$\tilde{H}_n(\lambda) = \tilde{G}_n(\lambda)\,\mathrm{arccot}\lambda - \tilde{K}_n(\lambda),$$

with

$$\tilde{K}_n(\lambda) = \sum_{k=1}^{\{n\}}(-1)^{k+1}\frac{2n-4k+1}{(2k-1)(n-k)}\left[1-\frac{(2k-1)(n-k)}{n(n-1)}\right]\tilde{G}_{n-2k+1}(\lambda)$$

where $\{n\} = n/2$ for even n, and $\{n\} = (n+1)/2$ for odd n.

Appendix C. Derivation of (69)

As stated in Happel & Brenner (1965), the expansion of a function $f(\mu)$ in a series with the Gegenbauer functions is as follows:

$$f(\mu) = \sum_{n=2}^{\infty} q_n\, G_n(\mu), \quad q_n = \tfrac{1}{2}n(n-1)(2n-1)\int_{-1}^{1}\frac{f(\mu)\,G_n(\mu)}{1-\mu^2}\,\mathrm{d}\mu. \tag{C 1}$$

Thus, to expand the right-hand side of the second condition (35), we need the following integrals:

$$I_{1n}(\lambda_0) = \int_{-1}^{1}\frac{\mu\,G_n(\mu)}{\lambda_0^2+\mu^2}\,\mathrm{d}\mu, \qquad I_{2n}(\lambda_0) = \int_{-1}^{1}\frac{\mu\,(1-\mu^2)\,G_n(\mu)}{\left(\lambda_0^2+\mu^2\right)^2}\,\mathrm{d}\mu.$$

The second integral is readily reduced to the first one as

$$I_{2n}(\lambda_0) = -\frac{1+\lambda_0^2}{2\lambda_0}\frac{\mathrm{d}I_{1n}}{\mathrm{d}\lambda_0} - I_{1n}(\lambda_0).$$

Thus, it remains to find $I_{1n}(\lambda_0)$. The integral is evaluated by using (54), and by resorting to the properties (see Abramowitz & Stegun 1965)

$$\int_{-1}^{1}\frac{P_n(\mu)}{\xi-\mu}\,\mathrm{d}\mu = 2\,Q_n(\xi), \qquad Q_n(-\xi) = -(-1)^n\,Q_n(\xi),$$

where ξ is a complex number outside the real interval $[-1, 1]$. We deduce

$$I_{1n}(\lambda_0) = -[1+(-1)^{n-1}]\,H_n(\mathrm{i}\lambda_0) = [1+(-1)^{n-1}]\,\mathrm{i}^{n-1}\,\tilde{H}_n(\lambda_0)$$

where the notation (56) has been used. Working back through the above derivation, we finally obtain (67) and (69).

REFERENCES

Abramowitz, M. & Stegun, I. A. (Eds.) 1965 *Handbook of Mathematical Functions*. Dover.

Akatnov, N. I. 1953 Development of two-dimensional laminar incompressible jet near a rigid wall. *Proc. Leningrad Polytec. Inst.* **5**, 24–31.

Amin, N. & Riley, N. 1990 Streaming from a sphere due to a pulsating source. *J. Fluid Mech.* **210**, 459–473.

Andrade, E. N. 1931 On the circulation caused by the vibration of air in a tube. *Proc. R. Soc. Lond.* A **134**, 445–470.

Banks, W. H. H. 1983 Similarity solutions of the boundary-layer equations for a stretching wall. *J. Méc. Théor. Appl.* **2**, 375–392.

https://doi.org/10.1017/S0022112003007122 Published online by Cambridge University Press

Davidson, B. J. 1973 Heat transfer from a vibrating circular cylinder. *Intl J. Heat Mass Transfer* **16**, 1703–1727.

Davidson, B. J. & Riley, N. 1972 Jets induced by oscillatory motion. *J. Fluid Mech.* **53**, 287–303.

Glauert, M. B. 1956 The wall jet. *J. Fluid Mech.* **1**, 625–643.

Gopinath, A. & Mills, A. F. 1993 Convective heat transfer from a sphere due to acoustic streaming. *Trans. ASME: J. Heat Transfer* **115**, 332–341.

Happel, J. & Brenner, H. 1965 *Low Reynolds Number Hydrodynamics*. Prentice-Hall.

Lee, C. P. & Wang, T. G. 1990 Outer acoustic streaming. *J. Acoust. Soc. Am.* **88**, 2367–2375.

Lee, C. P., Anikumar, A. V. & Wang, T. G. 1994 Static shape of an acoustically levitated drop with wave-drop interaction. *Phys. Fluids* **6**, 3554–3566.

Nyborg, W. L. 1965 Acoustic streaming. In *Physical Acoustics. Principles and Methods* (ed. W. P. Mason), vol. 2, part B, pp. 265–331. Academic.

Rayleigh, Lord 1883 On the circulation of air observed in Kundt's tubes and some allied acoustical problems. *Phil. Trans. R. Soc. Lond.* A **175**, 1–21.

Rednikov, A. & Riley, N. 2002 A simulation of streaming flows associated with acoustic levitators. *Phys. Fluids* **14**, 1502–1510.

Riley, N. 1965 Oscillating viscous flows. *Mathematica* **12**, 161–175.

Riley, N. 1966 On a sphere oscillating in a viscous fluid. *Q. J. Mech. Appl. Maths* **19**, 461–472.

Riley, N. 1967 Oscillatory viscous flows: review and extension. *J. Inst. Math Applics.* **3**, 419–434.

Riley, N. 1975 The steady streaming induced by a vibrating cylinder. *J. Fluid Mech.* **68**, 801–812.

Riley, N. 2001 Steady streaming. *Annu. Rev. Fluid Mech.* **33**, 43–65.

Riley, N. & Wybrow, M. F. 1995 The flow induced by the torsional oscillations of an elliptic cylinder. *J. Fluid Mech.* **290**, 279–298.

Sampson, R. A. 1891 On Stokes's current function. *Phil. Trans. R. Soc. Lond.* A **182**, 449–518.

Schlichting, H. 1932 Berechnung ebener periodischer Grenzchichtströmungen. *Phys. Z.* **33**, 327–335.

Schlichting, H. 1979 *Boundary-layer Theory*. McGraw-Hill.

Stuart, J. T. 1966 Double boundary layers in oscillatory viscous flows. *J. Fluid Mech.* **24**, 673–687.

Trinh, E. H. & Robey, J. L. 1994 Experimental study of streaming flows associated with ultrasonic levitators. *Phys. Fluids* **6**, 3567–3579.

Yarin, A. L., Brenn, G., Kastner, O., Rensink, D. & Tropea, C. 1999 Evaporation of acoustically levitated droplets. *J. Fluid Mech.* **399**, 151–204.

Yarin, A. L., Pfaffenlehner, M. & Tropea, C. 1998 On the acoustic levitation of droplets. *J. Fluid Mech.* **356**, 65–91.

Zhao, H., Sadhal, S. S. & Trinh, E. H. 1999*a* Singular perturbation analysis of an acoustically levitated sphere: flow about the velocity node. *J. Acoust. Soc. Am.* **106**, 589–595.

Zhao, H., Sadhal, S. S. & Trinh, E. H. 1999*b* Internal circulation in a drop in an acoustic field. *J. Acoust. Soc. Am.* **106**, 3289–3295.

https://doi.org/10.1017/S0022112003007122 Published online by Cambridge University Press